

12-2017

Development of a Remotely-Piloted Vehicle Platform to Support Implementation, Verification, and Validation of Pilot Control Systems

Sean O'Toole

Follow this and additional works at: <https://commons.erau.edu/edt>



Part of the [Aerospace Engineering Commons](#)

Scholarly Commons Citation

O'Toole, Sean, "Development of a Remotely-Piloted Vehicle Platform to Support Implementation, Verification, and Validation of Pilot Control Systems" (2017). *Dissertations and Theses*. 372.
<https://commons.erau.edu/edt/372>

This Thesis - Open Access is brought to you for free and open access by Scholarly Commons. It has been accepted for inclusion in Dissertations and Theses by an authorized administrator of Scholarly Commons. For more information, please contact commons@erau.edu.

DEVELOPMENT OF A REMOTELY-PILOTED VEHICLE PLATFORM TO
SUPPORT IMPLEMENTATION, VERIFICATION, AND VALIDATION OF PILOT
CONTROL SYSTEMS

A Thesis

Submitted to the Faculty

of

Embry-Riddle Aeronautical University

by

Sean O'Toole

In Partial Fulfillment of the

Requirements for the Degree

of

Master of Science in Aerospace Engineering

December 2017

Embry-Riddle Aeronautical University

Daytona Beach, Florida

DEVELOPMENT OF A REMOTELY-PILOTED VEHICLE PLATFORM TO
SUPPORT IMPLEMENTATION, VERIFICATION, AND VALIDATION OF PILOT
CONTROL SYSTEMS

by

Sean O'Toole

A Thesis prepared under the direction of the candidate's committee chairman, Dr. Hever Moncayo, Department of Aerospace Engineering, and has been approved by the members of the thesis committee. It was submitted to the School of Graduate Studies and Research and was accepted in partial fulfillment of the requirements for the degree of Master of Science in Aerospace Engineering.

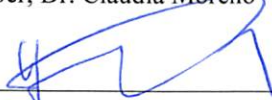
THESIS COMMITTEE



Chairman, Dr. Hever Moncayo



Member, Dr. Claudia Moreno



Member, Dr. Yan Tang



Graduate Program Coordinator, Dr. Magdy Attia



Dean of College of Engineering, Dr. Maj Mirmirani



Vice Chancellor, Academic Support, Dr. Christopher Grant

12-7-2017

Date

12/7/2017

Date

12/7/17

Date

ACKNOWLEDGMENTS

It is with great honor that I can thank all those who provided support and assistance in this process of completing a thesis study. First off, I would like to thank my mother and father, Debbie & Tim O'Toole. They have always provided me with unconditional love, support and inspiration. They have been role models to me, taught me a lot about life, and helped me become the man I am today. I would also like to thank my wife, Angelia, for her love, devotion and patients in this process as many late night and lots of time has been spent on this research.

Dr. Hever Moncayo, I would like to thank you for taking me under your advice and providing guidance in this research topic. In the last three years you have taught me a lot about dynamics and controls and I appreciate you accepting me into the Flight Dynamics and Controls Research Lab. I have made many friends and enjoyed becoming a part of the dynamics and control family! Additionally, my appreciation for my thesis' committee members, Dr. Yan Tang and Dr. Claudia Moreno, for their valuable input towards the completion of this manuscript.

For all those whom I had the opportunity to work with and alongside, thank you, especially to my friends in the FDCRL; you all were there whenever a hand was needed. Special thanks to Yomary Betancur and Cindy Nshuti who helped tremendously when there were technical difficulties. Nolan Coulter, your friendship made the whole process more enjoyable, and I will miss having you as a neighbor in the lab. To the Pilots Eric Frantz, Robert Moore, and Albert Obi your time and efforts at the airfield are much appreciated. Lastly and most importantly I would like to give the glory to God! For he is the one who opened the doors and gave me the ability to succeed and endure.

TABLE OF CONTENTS

LIST OF TABLES	vi
LIST OF FIGURES	vii
SYMBOLS.....	ix
ABBREVIATIONS	x
ABSTRACT.....	xi
1. Introduction.....	1
1.1. Literature Review	2
1.1.1. Pilot-Induced Oscillations.....	2
1.1.2. Testbed Platforms.....	4
1.1.3. Metrics for Evaluation of Handling Qualities and PIO.....	5
2. Remotely – Piloted Vehicle Platform	7
2.1. Hardware.....	8
2.2. Software	17
2.2.1. Simulink Real-Time	17
2.2.2. PX4 Support Package.....	18
3. Simulation Environment.....	20
3.1. Equations of Motion.....	21
3.2. Aircraft Dynamics	24
3.3. Actuator Dynamics.....	25
3.4. Aircraft Failure Model	26
3.5. Control Architectures	27
3.5.1. Pilot Reference Model.....	28
3.5.2. Non-Linear Dynamic Inversion.....	29
4. Pilot Induced Oscillation Metrics	33
4.1. Pilot Modeling	35
4.2. Flying Qualities and PIO Criterion	37
5. Results.....	41
5.1. Simulation Experiments.....	41
5.2. Flight Testing	51
6. Conclusion and Future Work.....	55
REFERENCES	57

LIST OF TABLES

Table 2.1 SIG Rascal 110 Geometric Data	14
Table 3.1 Preliminary Stability Derivatives from Digital Datcom	24
Table 3.2 Trim Conditions for Rascal in Simulation	25
Table 4.1 Cooper-Harper Rating Scale (Cooper, G. and Harper, R. 1969)	39
Table 5.1 Trim conditions for RPV simulation	41
Table 5.2 Optimized Kp, TL with $\angle pc$, and $rms\theta e$	42
Table 5.3 Pilot-in-the-Loop Experiments	47

LIST OF FIGURES

Figure 1.1 Closed Loop Pitch Attitude Control Task Schematic Diagram (Bailey, R. and Bidlack, T. 1996)	5
Figure 2.1 SIG Rascal 110 with all systems installed.....	7
Figure 2.2 ERAU Mobil Ground Station.....	8
Figure 2.3 PCM-3355 Enclosure with input/output ports.....	9
Figure 2.4 LORD MicroStrain® 3DM-GX4-45™	9
Figure 2.5 Pixhawk passing through RS-232 to TTL converter and into PCM-3355	10
Figure 2.6 Multiplexer (bottom left) connected to AR8000 receiver (top left and right). ..	11
Figure 2.7 AXi 5345/18HD mounted on Rascal.....	12
Figure 2.8 FPV Camera (left), HUD visual and MRM OSD (center), Boscam video transmitter with Immersion clover antenna (right)	13
Figure 2.9 Ground Station Pilot Cockpit	15
Figure 2.10 RPV and Ground Station Signal/Power scheme	16
Figure 2.11 Simulink Real-Time Compilation Steps.....	17
Figure 2.12 Pixhawk Simulink Library	19
Figure 3.1 Simulation pilot cockpit in lab	20
Figure 3.2 6-DoF aircraft body axis.....	21
Figure 3.3 Elevator system response to a step input of 25° (Lyons, B. 2013).....	25
Figure 3.4 Motor System Thrust Response to 5.75 lbs. input (Lyons, B. 2013)	26
Figure 3.5 Failure setup graphical user interface (GUI)	27
Figure 3.6 General Simulation Architecture	30
Figure 4.1 Performance Optimization Plot	35
Figure 4.2 Optimization Tool Box.....	37
Figure 4.3 Time-Domain Neal-Smith Parameter Plane.....	38
Figure 4.4 Time-Domain Neal-Smith PIO parameter plane.....	40
Figure 5.1 Nominal handling qualities and PIO prediction	43
Figure 5.2 Optimization Tracking for D=2.25sec NLDI (Left) Stick-to-Servo (Right)...	44
Figure 5.3 Delay 300ms handling qualities and PIO prediction.....	44
Figure 5.4 NLDI experiences PIO when a delay of 300ms present and performing an aggressive maneuver (D=1.25)	45
Figure 5.5 Right Aileron Lock at 2° handling qualities and PIO prediction.....	45
Figure 5.6 HUD used by pilot to acquire maneuver	46

Figure 5.7 Audio and Visual Cue for Pilot to Start and Complete Maneuver	46
Figure 5.8 Nominal Pilot-in-the-Loop Time-Domain Handling Qualities	49
Figure 5.9 Pilot-in-the-Loop with 300ms Delay Stick-to-Servo (left) NLDI (right).....	50
Figure 5.10 300ms Delay Pilot-in-the-Loop Time-Domain Handling Qualities	50
Figure 5.11 2° Right Aileron Lock Pilot-in-the-Loop Time-Domain Handling Qualities	51
Figure 5.12 Daytona RC Flying Park	51
Figure 5.13 Flight Test at Daytona RC Flying Park	54

SYMBOLS

m	Mass
v	Velocity
\angle_{pc}	Pilot phase compensation angle
p, q, r	Roll rate, pitch rate, yaw rate
I_{xx}, I_{yy}, I_{zz}	Symmetrical moments of inertia
u, v, w	Linear velocities
ϕ, θ, ψ	Euler angles
$\dot{\phi}, \dot{\theta}, \dot{\psi}$	Euler rates
θ_c	Commanded pitch
α	Angle of attack
β	Angle of side-slip
\vec{F}	Vector of total forces
\vec{M}	Vector of total moments
$p_{com}, q_{com}, r_{com}$	Roll, pitch, and yaw rate command
ω_n	Natural frequency
ζ	Damping
ω_{BW}	Bandwidth frequency
$rms(\theta_e)$	Root-mean-squared pitch error
$\dot{x}, \dot{y}, \dot{z}$	Inertial reference frame velocities

ABBREVIATIONS

RPV	Remote-Pilot Vehicle
GCS	Ground Control Station
UAV	Unmanned Aerial Vehicle
PIO	Pilot-Induced Oscillation
AirSTAR	Airborne Subscale Transport Aircraft Research
NASA	National Aeronautics and Space Association
WVU	West Virginia University
ADCL	Advanced Dynamics and Control Lab
TTL	Transistor-Transistor Logic
PWM	Pulse Width Modulation
FPV	First-Person Viewer
OSD	On-Screen Display
APC	Advanced Precision Composites
Li-Po	Lithium Polymer
Ni-MH	Nickel-Metal Hydride
ESC	Electronic Speed Controller
MAC	Mean Aerodynamic Chord
IMU	Inertial Measurement Unit
INS	Inertial Navigation System
6-DoF	Six-Degree of Freedom
NLDI	Non-Linear Dynamic Inversion
DCM	Direct Cosine Matrix
GUI	Graphical User Interface
PI	Proportional-Integral

ABSTRACT

O'Toole, Sean MSAE, Embry-Riddle Aeronautical University, December 2017.
Development of a Remotely-Piloted Vehicle Platform to Support Implementation,
Verification and Validation of Pilot Control Systems.

This thesis presents the development of a research test bed and the use of a set of metrics for evaluating handling qualities with pilot in the loop configuration. The main objective of this study is to provide software and hardware tools to support performance evaluation of control systems designed to compensate for Pilot Induced Oscillations (PIOs). A remotely-piloted vehicle presented in this thesis consists of an RC aircraft modified to be flown from a ground station cockpit. The unmanned aerial system has a high-speed on-board processing system capable of simulating different conditions during flight such as injecting actuator failures and adding delays. In this study, the analysis of pilot handling qualities based on a set of evaluation metrics, is also included. The metrics are based on time-domain Neal-Smith criterion and are used to provide numerical data which categorizes the control system in one of the levels on the Cooper-Harper Rating scale. Two different control configurations were implemented and analyzed in this study: stick-to-servo and non-linear dynamic inversion control laws. Piloted-simulation results are presented on the Neal-Smith flying qualities plane at different flight conditions.

1. Introduction

Most current and future aircraft are or will be utilizing fly-by-wire technology, which allows for implementation of control systems to aid the pilot during operation. One major focus of the National Aeronautics and Space Administration (NASA) Aviation Safety Program is the research of transport-category aircraft during adverse flight conditions such as upsets, damage, and failures (Murch, A., 2008). When an aircraft is under adverse conditions it can lead to unfavorable pilot-vehicle interaction, loss of control, and ultimately catastrophe. These loss of control events go “beyond the normal flight envelope into regions where aerodynamic data is not available from conventional sources” (Jordan, T. L., et. al., 2006). In an effort to safely assist with the development of methods to minimize loss of control events, several type of Remotely Piloted Vehicle (RPV) platforms have been developed.

RPV platforms have provided a safe and cost-efficient option towards the research in loss of control events. They allow for rapid development, testing and validation of flight controllers within these loss of control regions that are outside the normal flight envelope. Additionally, different categories of failures can be simulated in this test bed environment and pilot-vehicle interaction can be observed.

During the testing and validation, it is necessary to evaluate the handling qualities of the control system. Since RPVs, do not have the motion cues like manned aircraft a metric is necessary for true evaluation of the handling. According to researchers at the University of Illinois at Urbana-Champaign:

Prediction of flying qualities and adverse aircraft-pilot coupling, fundamentally characterized by the closed-loop aircraft-pilot interactions, has remained as one of the key (missing) steps towards the application of adaptive control technologies in manned (and unmanned) aircraft (Choe, Ronald, et. al., 2010).

The handling qualities can be representative of the pilot's ability to "acquire the target quickly, and predictably with a minimum of overshoot and oscillation" (Choe, R., et. al. 2010). Methods for evaluation and detection are based either in frequency- or time-domain. The current criteria recognized for handling qualities uses the frequency-domain and is contained in Military Specification (MIL-STD-1797). During the evaluation of handling qualities one adverse pilot-vehicle interaction which can be detected, is pilot induced oscillation. Systems which is susceptible to pilot induced oscillation, or PIO, is known as PIO-prone. There are a few methods used in evaluation of PIOs: Smith-Geddes criterion, Open Loop Onset Point method, and Neal-Smith criterion.

This thesis uses the time-domain Neal-Smith criterion which has been shown in previous research by (Bailey, R. and Bidlack, T. 1996) to be equivalent to the frequency-domain criteria for analysis of flying qualities. The time-domain Neal-Smith criteria, at its foundation, is a combination of the frequency-domain Neal-Smith criteria and step target tracking criteria (Bailey, R. and Bidlack, T. 1995). Through using the time-domain, analysis of all systems can be done without the need to make assumptions on linearity, inferred pilot inputs or control activity. This proves useful when an aircraft is under certain failures, as the system typically becomes nonlinear. The time-domain Neal-Smith criterion is utilized to analyze two configurations in this thesis. The standard stick-to-servo where no controller is augmented with the pilot, and the other configuration utilizes a non-linear dynamic inversion controller.

In Chapter 2 of this thesis, the development and assembly of the RPV is addressed with

details and descriptions of the hardware and software which is used onboard and in the Ground Control Station (GCS). Chapter 3 explains how the vehicle is modeled for simulation, and the different controllers which are used to provide comparison when evaluating handling qualities. The way handling qualities metric is formulated and how it can be used to predict pilot-induced oscillations is discussed in Chapter 4. Chapter 5 outlines the experiments which were conducted for pilot-in-the-loop simulation. Additionally, the results from the pilot-in-the-loop simulation experiments and flight test are presented in the fifth chapter. Lastly to conclude this thesis an overall conclusion and preamble to future work and suggestions are made in Chapter 6. The two main objectives of this thesis are:

1. Development of a remotely-piloted vehicle platform which can be flown from a ground control station cockpit
2. Pilot-in-the-loop simulation utilizing the time-domain Neal-Smith criterion for the evaluation of handling qualities and PIO tendencies under nominal and failure conditions.

1.1. Literature Review

1.1.1. Pilot-Induced Oscillations

Aircraft loss of control is one of the leading factors in the cause of fatal accidents. From the time of 2006 through 2015 there were 15 large commercial jet airplane accidents that resulted in 1396 fatalities (Belcastro, C.M. et. al. 2017). Loss of control is defined as motion that is outside the normal operating flight envelope; not predictably but altered by pilot control inputs; characterized by nonlinear effects, such as kinematic/inertial coupling, disproportionately large responses to small state variable changes, or oscillator/divergent

behavior; likely to result in high angular rates and displacements; characterized by the inability to maintain heading, altitude, and wings level (Wilborn, J.E., Foster, J.V. 2004). In a study performed by (Belcastro, C.M. et. al. 2017) their statistics for loss of control found aggressive maneuvers and abnormal maneuvers accounted for 5% and 9% of occurrences, respectively.

Aggressive maneuvers or improper maneuvers are one of the cases which can lead to PIO, a subcategory in loss of control. PIO is defined as the sustained or uncontrollable oscillations resulting from the pilot's efforts to control the aircraft. High profile PIO incidents involving the Lockheed/Boeing/General Dynamics YF-22 and SAAB JAS-39 show that it is important to understand what causes PIO and how to prevent it (Mandal, Tanmay, et. al. 2013).

PIO's are typically labeled in three different categories. This thesis only focuses on category I and II failures to test in simulation. These categories as described in (Mcruer, D., et. al. 1997) are:

Category I: This category is a linear pilot-vehicle system oscillation. The aircraft can be characterized by a linear function, and the pilot acts as a linear transfer function where the inputs are sinusoidal and neither the aircraft nor pilot's dynamics change during PIO. The aircraft gains are a major factor in PIO where too high of gain makes for high sensitivity and too low of gains makes for sluggish responses. Not all category I PIOs are severe. Faulty pilot adaptation is a typical case of category I PIO but can be negated as more familiarity of the aircraft's characteristics is gained. However, those PIOs where the gain range is inadequate or there is excessive time delay will not go away and can lead to catastrophe.

Category II: This category consists of rate and position limiting with a quasi-linear pilot-vehicle system oscillation. These are severe oscillations with high amplitudes where rate and position limits prevent recovery. They are the most common aircraft pilot coupling event, and typically occur with little or no notice (Mandal, Tanmay, et. al. 2013).

1.1.2. Testbed Platforms

Testbed platforms allow for actual flight test to be conducted, which is necessary when attempting to understand the complex and relatively unexplored nature of transport aircraft dynamics during event that lead to loss of control (Murch, A. 2008). Research efforts towards the development of mobile test-beds that can be used to investigate adverse flight conditions such as upsets, damage, and failures are being conducted by scholars at NASA and West Virginia University (WVU). NASA and WVU both have developed GCS that utilize low cost, easy-fly and maintain, robust platforms that are capable of hosting research data and control systems (Jordan, T. L., Bailey, R. M. 2008).

The Airborne Subscale Transport Aircraft Research (AirSTAR) testbed of NASA Langley Research Center has been leading the way with focuses on aviation safety research (Guerra, M., et. al., 2012). Their ground control station hosts three stations: a flight research station, operations command station, and operations engineering station. An additional external area is the safety pilot station. These stations all work together to enable the test flights of multiple unmanned aerial vehicles (UAVs), ranging from expensive, custom-built, scale model aircraft to off the shelf radio controlled planes, which can be used interchangeably.

West Virginia University's testbed platform is like that of NASA's AirSTAR although much more affordable. Their GCS is made from a box truck that has been modified to

accommodate necessary equipment to fly and collect data with their UAV. Their UAV is a custom-built aircraft called the “Phastball,” and host avionics for measuring the aircraft states and providing video to the GCS pilot. WVU’s UAV is capable of autonomous or partially autonomous flight from either the GCS or with an RC pilot.

1.1.3. Metrics for Evaluation of Handling Qualities and PIO

The evaluation of flying qualities can either be done in the frequency-domain or the time-domain. Both frequency- and time-domain performance analyze the systems closed-loop response. Closed-loop means a state is fed back through to compare to a commanded or desired state, the error is then passed through a pilot transfer function which attempts to bring the error to zero (Figure 1.1).

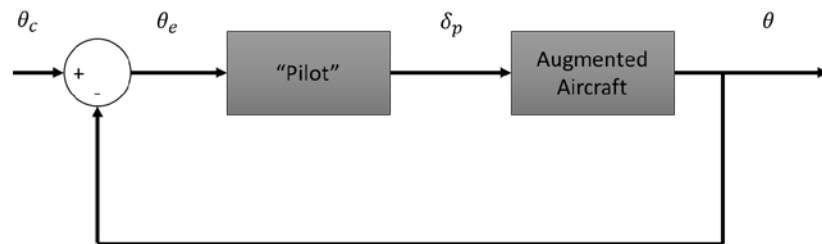


Figure 1.1 Closed Loop Pitch Attitude Control Task Schematic Diagram (Bailey, R. and Bidlack, T. 1996)

The frequency-domain Neal-Smith criteria is based on different task demands which are defined by the bandwidth frequency. The pilot’s workload is then represented by the phase compensation angle at the bandwidth frequency, \angle_{pc} , and compares it with the closed-loop resonance, $\left| \frac{\theta}{\theta_c} \right|$. The closed loop resonance is representative of the pilot’s ability to accurately acquire the task. One shortfall of this method is that it is “not necessarily adequate for the analysis of nonlinear flight control system elements” (Bailey,

R. and Bidlack, T. 1996). The reason for this is because frequency-domain cannot account for non-linearities without making assumptions and estimations.

The time-domain Neal-Smith criteria is another method that can be used to investigate handling qualities. It stems from the frequency-domain Neal-Smith criterion (Choe, R. et. al. 2010). In a similar way to the frequency-domain, the task demands are defined by the task acquisition time. The ability for the control system to track the desired or commanded state is represented by the root-mean-squared value of the tracking error. Lastly, the pilot work load, like that of the frequency-domain, is represented by the pilot phase compensation angle. In previous study by (Bailey, R. E. and Bidlack, T. J., 1996) the time-domain Neal-Smith criterion showed promising quantitative criterion for the prediction of flying qualities and Pilot Induced Oscillation (PIO) tendencies.

Both the frequency- and time-domain Neal-Smith Criterion define PIO-prone configurations as those systems that are susceptible to more error due to changes in the aggressiveness of a maneuver.

2. Remotely – Piloted Vehicle Platform

Large RC hobby planes have the capability to host avionics and can be easily modified to meet research criteria. They are low-cost, easily maintained platforms. NASA utilizes different types of commercial-off-the-shelf transport models to allow for rapid evaluation of control design concepts (Jordan, T., Bailey, R. 2008).

Here in the Advanced Dynamics and Control Lab (ADCL) at Embry-Riddle Aeronautical University the SIG Rascal 110 RC hobby plane, Figure 2.1, is used in conjunction with a portable closed trailer, Figure 2.2, to create the RPV platform. The Rascal was chosen as the airframe due to its large size and ability to house the needed hardware with only minor modification. Additionally, the SIG Rascal 110 has also been used by several other institutions as a research airframe (Choon Seong, 2008) (Xargay, E., et. al., 2013).



Figure 2.1 SIG Rascal 110 with all systems installed



Figure 2.2 ERAU Mobil Ground Station

The trailer chosen for the ground station is a custom-built trailer from Pace American. It was custom built to allow for climate control, power outlets, and a circuit breaker which can be powered by a generator or outlet. The trailer had further customization by installing desk and shelving to allow for workstations and a place to secure aircrafts for transport. In the following subsections both the aircraft and ground station are discussed, first addressing the embedded 1) Hardware and then 2) Software.

2.1. Hardware

To have the SIG Rascal 110 operation for the purposes of this study, motors, servos, a microcontroller, computer, and several sensors were installed. Most important of these was the PCM-3355 by Advantech. This is a small PC-104 type computer that can be stacked with other boards to perform necessary processes. The PCM-3355 is the primary computer of the RPV. It gives the vehicle the ability to process and save large amounts of data, and can be used to run real-time simulation. The system features an AMD LX800/500 MHz and LX600/366 MHz processor by Geode™. Also included are two RS-232 port and two

USB 2.0 ports. In addition to the use of the PCM-3355, an Emerald-MM-4M by Diamond Systems® was stacked on top to provide an additional 4 serial ports. The computer stack was assembled and then placed inside a 3D printed enclosure with input/output ports to allow for external devices to be easily connected to the PCM-3355, see Figure 2.3.



Figure 2.3 PCM-3355 Enclosure with input/output ports

MicroStrain® 3DM-GX4-45™ INS as shown in Figure 2.4 is one of the sensors that is read by the PCM-3355 on-board the RPV. This sensor provides highly accurate measurements of the aircraft attitude ($\pm 0.8^\circ$), angular rates, and accelerations. It uses an Extended Kalman Filter to provide more accurate results and, to compute GPS location ($\pm 5\text{m}$), velocities ($\pm 0.1\text{m/s}$) as well as pressure altitude. This sensor is selected for its ease of use, light weight, high accuracy, and performance. The MicroStrain® automatically compensates for vehicle noise and vibration, and does not need field calibration due to automatic magnetometer calibration and anomaly rejection.



Figure 2.4 LORD MicroStrain® 3DM-GX4-45™

Pixhawk by 3D Robotics™ is a micro controller that is used in this thesis to read pulse width modulation (PWM) signals from the remote-control inputs and send them through the serial port. Pixhawk also has a built in IMU and barometer which is primarily used as a redundant system to back up better quality hardware as described earlier. However, before the values measured by the Pixhawk can be read by the PCM-3355 it must first go through a RS-232 to transistor-transistor logic (TTL) converter (Figure 2.5). This is because Pixhawk communicates in TTL which is a binary logic that uses voltages between 0V and +5V while RS-232 port on most PCs typically read voltages from -13V to +13V. The RS-232 to TTL converter changes voltages so that the two systems can communicate.

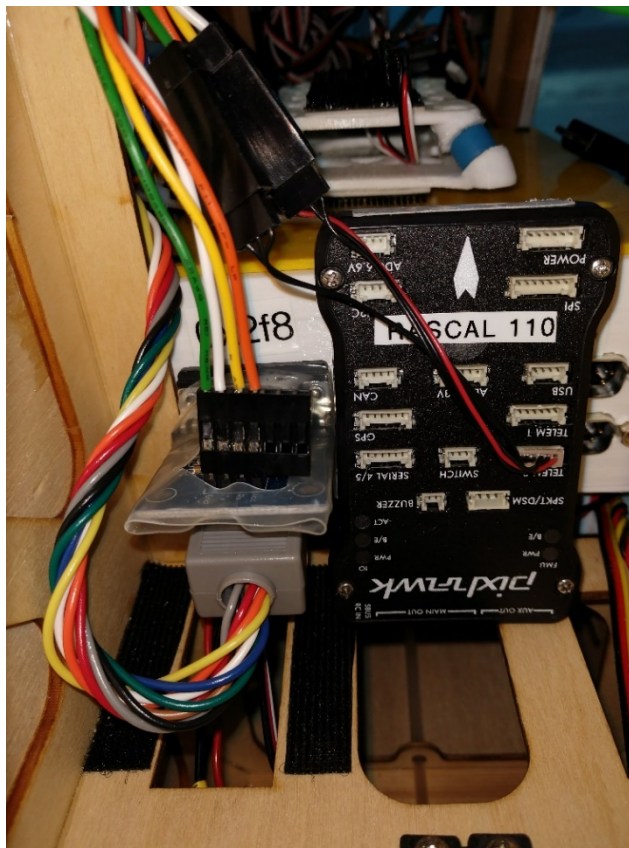


Figure 2.5 Pixhawk passing through RS-232 to TTL converter and into PCM-3355

Polulu Mini Maestro 18 is a servo controller which also uses an RS-232 to TTL converter. The Polulu reads the RS-232 signal from the PCM-3355 and converts it to a PWM signal which can actuate the servos on the RPV with a resolution of $0.25\mu\text{s}$.

The Transmitter used to by the RC pilot is a Spektrum DX7 7-channel receiver. This transmitter is used due to its many channels and ability to be set up in wireless trainer mode which is used to switch control to the ground station pilot. The transmitter is connected to an AR8000 8-channel receiver by Spektrum. This receiver is used because of its redundancy of two receivers which reduces the chances of a lost connection. The receiver obtains the signal from the transmitter and then feeds the signal to both the Pixhawk and an 8-channel RC/RX multiplexer by Cytron Technologies as seen in Figure 2.6. This multiplexer is used to allow the RC pilot to switch from running the signals directly to the servos to running through the primary on-board computer. It is most useful as a fail-safe, by allowing the RC pilot to abort the test, regain control of the aircraft and land safely.

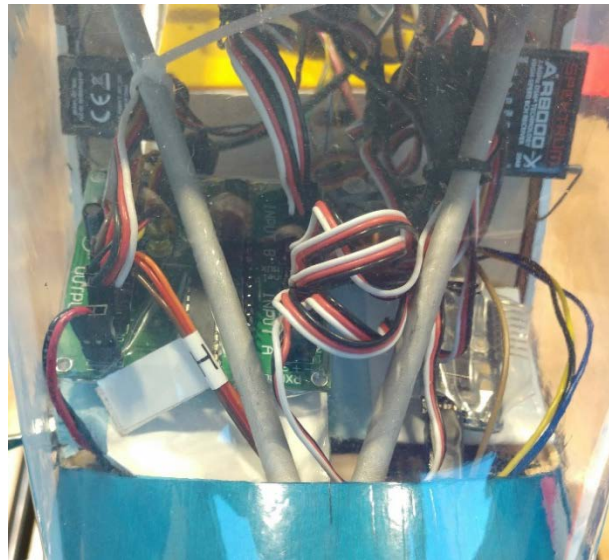


Figure 2.6 Multiplexer (bottom left) connected to AR8000 receiver (top left and right)

The actuators that were recommended and used on the Rascal 110 are the HS-5625MG Digital Servo by Hitec. It is a digital metal gear servo designed for high speed and high torque applications. There are in total 6 of these servos used for actuation: 1 for elevator, 2 for ailerons, 1 for rudder, and 2 for flaps.

Due to the increased weight and desire for a longer flight, the selected motor is an AXi 5345/18HD, as displayed in Figure 2.7, with a 20x13 propeller by Advanced Precision Composites (APC). The motor is a brushless DC motor that can draw up to 75 amps and operates at 171 Kv (171 RPM/V). It can handle up to a 12-cell lithium polymer (Li-Po) battery. The 20x13 APC propeller means it has a diameter of 20 inches and a pitch of 13 degrees at 25% of the length of the radius.



Figure 2.7 AXi 5345/18HD mounted on Rascal

The motor is controlled by an electronic speed controller (ESC), Jeti Spin 99 Pro Opto Brushless. This ESC can support a continuous draw of 99 amps and a max current draw of 109 amps. It is important that the proper ESC, motor, propeller, and battery combination is selected to meet the needs of the desired performance.

There are 4 batteries used on board the Rascal. Two 6-cell Li-Po batteries connected in series generate approximately 50V to power the AXi motor. The servos are powered by a

4-cell nickel-metal hydride (Ni-MH) battery that produces approximately 5V. There is an additional 3-cell Li-Po battery to power the camera, primary on-board computer, and video transmitter.

Providing video to the ground station pilot is done with the use of a First-Person Viewer (FPV) camera, MRM On-Screen Display (OSD), and Boscam 5.8 GHz video transmitter with an Immersion clover antenna, see Figure 2.8. The MRM OSD takes values from the Pixhawk IMU and barometer and overlays them on the video image from the FPV camera. The video with the OSD overlay (Figure 2.8 center) is then transmitted to the ground station receiver.

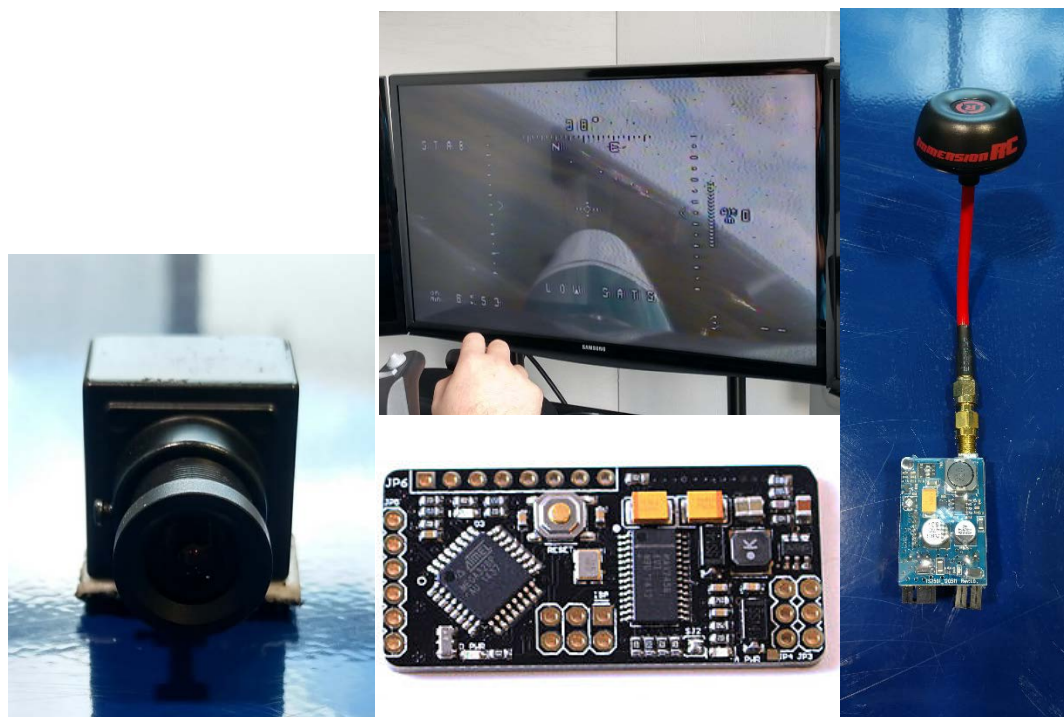


Figure 2.8 FPV Camera (left), HUD visual and MRM OSD (center), Boscam video transmitter with Immersion clover antenna (right)

All the new components added to modify the SIG Rascal 110 gives it the geometric properties shown in Table 2.1.

Table 2.1 SIG Rascal 110 Geometric Data

Parameter	Value
Mass	9.16 <i>kg</i>
Wingspan	2.80 <i>m</i>
Wing Area	0.981 <i>m</i> ²
MAC	0.351 <i>m</i>
I_{xx}	2.64 <i>kg · m</i> ²
I_{yy}	2.10 <i>kg · m</i> ²
I_{zz}	2.59 <i>kg · m</i> ²

The ground station is where data can be analyzed, and the pilot sits to fly the RPV. A pilot sits in a Volair Sim™ Cockpit which holds 3 monitors to provide visuals for the pilot (Figure 2.9). Hardware used to provide visuals to the pilot from the RPV is a Boscam 5.8GHz video receiver. Pilot inputs are commanded on a CH Eclipse yoke which is also shown in Figure 2.9. Inputs from the yoke are passed through to a ForceFly computer made by EMR Labs. ForceFly enables the yoke controls to be transmitted through the wired trainer port of a transmitter. A Spektrum DX5e transmitter is used, and wirelessly bound to the RC pilots DX8 transmitter.



Figure 2.9 Ground Station Pilot Cockpit

Two additional desktop computers are used for the engineer workstation and the weather station. Software is generated and able to be uploaded through ethernet cable onto the RPV prior to starting flight test from the engineer workstation. The weather station reads wind speed and direction from sensors placed outside the ground station. Figure 2.10 summarizes the power and signal flow for RPV and GCS.

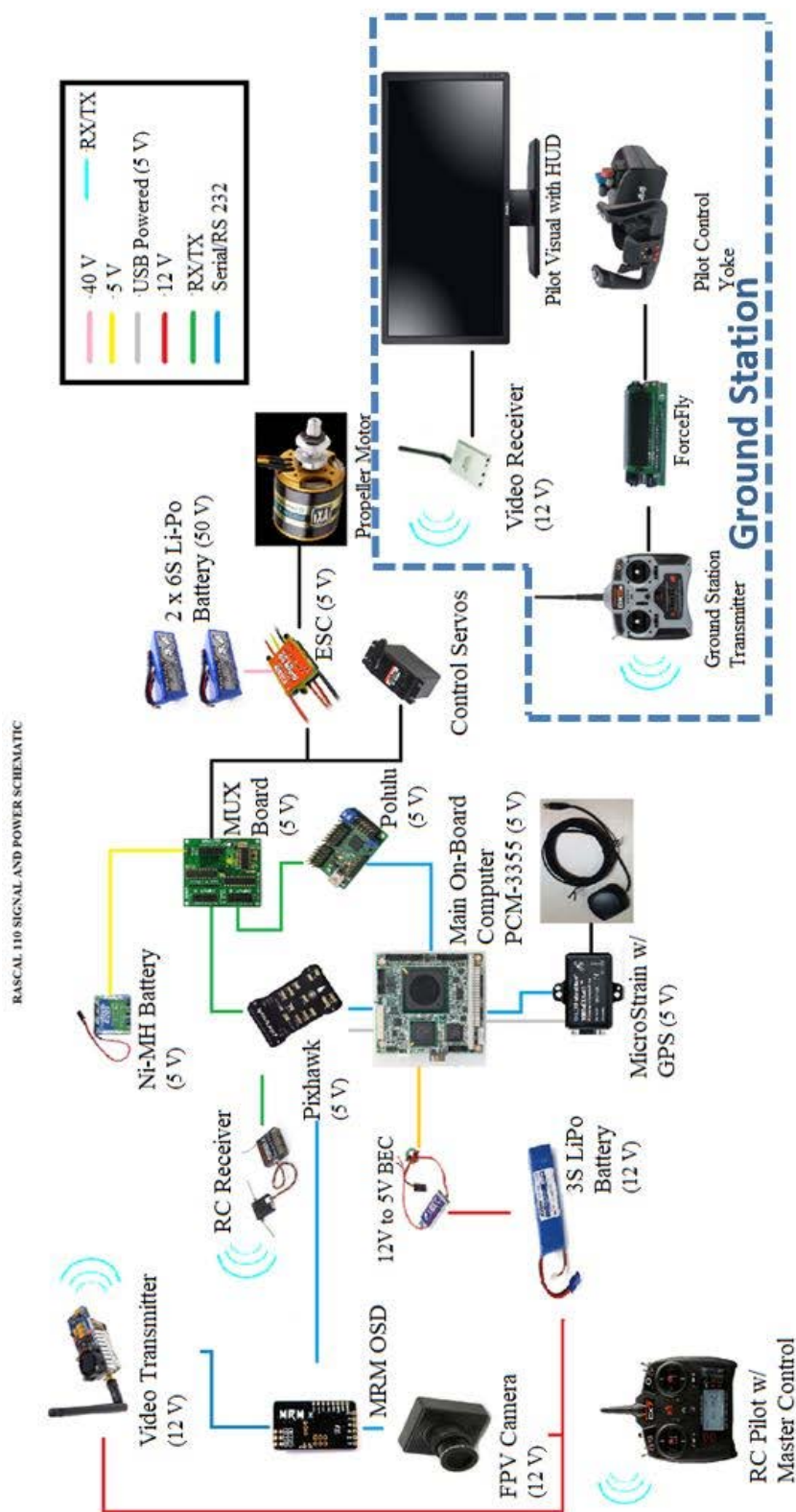


Figure 2.10 RPV and Ground Station Signal/Power scheme

2.2. Software

Software enables the sensors and controller to communicate with the RPV's on-board computer and allows the engineer station to choose which experiments are to be tested. In this thesis real-time applications are tested using MathWorks® MATLAB, Simulink and Simulink Real-Time™.

2.2.1. Simulink Real-Time

Simulink Real-Time™ allows real-time simulation and testing. “The typical environment for real-time applications consist of a development computer [engineer's station], and the hardware under test [RPV's on-board computer]” (MathWorks. 2017). Initialization code is built on the host computer in MATLAB to define states and values that are used in Simulink models. The target computer is connected to using a boot drive and TCP/IP protocol. The boot drive defines the targets IPv4 address so that the host may find it and connect. When the Simulink model is commanded to build to the target, the model passes through a C compiler which then builds onto the target computer (Figure 2.11).

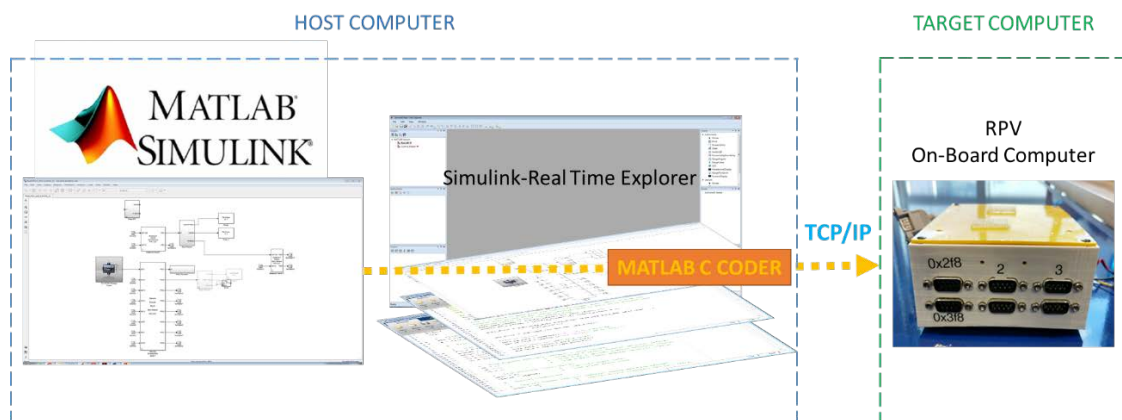


Figure 2.11 Simulink Real-Time Compilation Steps

The Simulink Real-Time Explore opened on the host computer allows management and control of the simulation that is built on the target computer. Additionally, the explorer can read data and scopes that are inserted in the Simulink model built on the target. These scopes are useful for collecting and storing data while the RPV is in flight. In the real-time Simulink library are blocks that are used to read RS-232 Serial ports. The receiving RS-232 blocks define the serial ports for the pixhawk, MicroStrain® and how many values are read. Headers are utilized to ensure that the information collected is in the proper order. RS-232 blocks are also used to send commands through the onboard computer to the Polulu which can move the servos.

2.2.2. PX4 Support Package

Simulink has many libraries for different hardware, but most useful for this thesis was their Pixhawk library (Figure 2.12). This library has blocks which enables Pixhawk to view values of signals and tune parameters in real time. The blocks also give Pixhawk the ability to log and record flight data of sensors, although not as much data as is capable by the PCM-3355. The main support blocks used in this thesis are those for reading PWM signals from the RC transmitters, in addition to reading IMU values and sending information through a selected I/O ports to be read by the RPVs on-board computer.

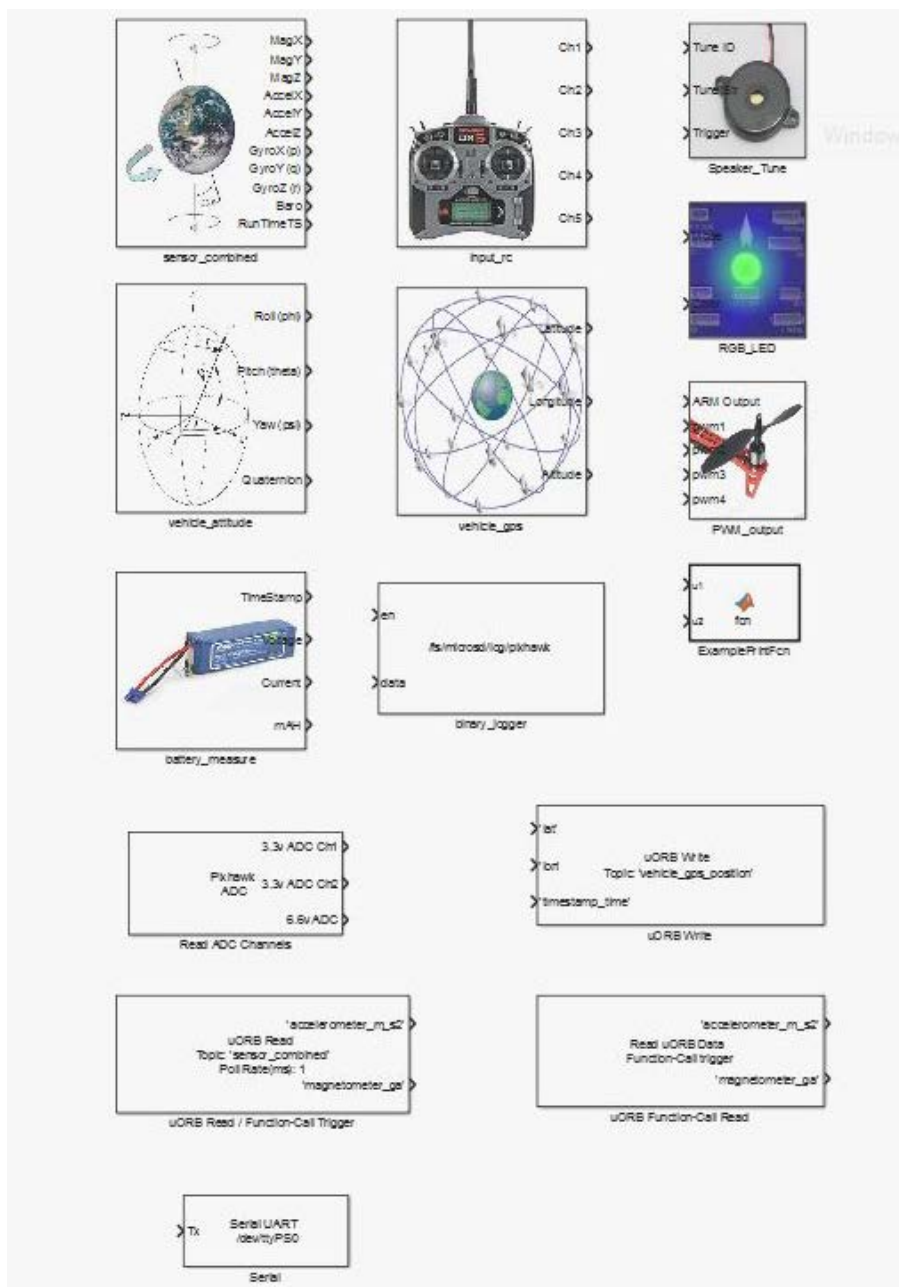


Figure 2.12 Pixhawk Simulink Library

3. Simulation Environment

The ultimate objective of this thesis is a full working RPV and GCS where flight controls can be tested. However, before performing real-time flight test it is necessary to conduct preliminary test of different controllers in simulation, and to train the pilot under manual and augmented control modes. Flight simulator lab setup has the same look and feel as that of the ground control station (Figure 3.1). MATLAB and Simulink are used to develop an environment that models the Rascal with the desired controllers. The visuals in simulation are provided through FlightGear v3.4.0.



Figure 3.1 Simulation pilot cockpit in lab

Further explanation on the equations of motion, modeling of the SIG Rascal 110, and controllers implemented are covered in the following subsections.

3.1. Equations of Motion

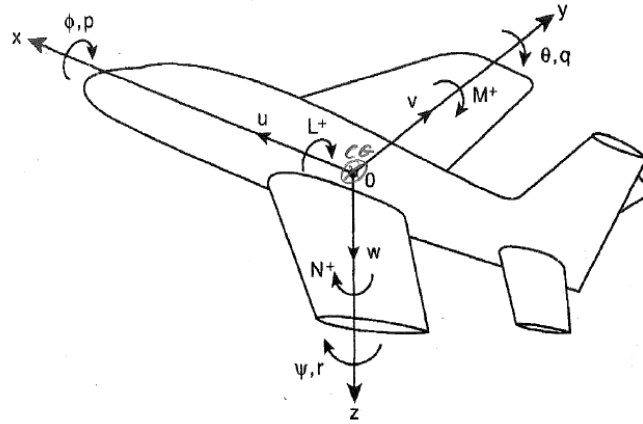


Figure 3.2 6-DoF aircraft body axis

Simulation of the RPV aircraft dynamics is done by utilizing a non-linear six-degree-of-freedom (6-DoF) set of equations of motion. Assumptions of a rigid-body RPV, and “flat-Earth equations ... [Earth-fixed], with constant gravity, are sufficient for aircraft simulation...” (Stevens, B. L., et. al., 2016). The 6-DoF model requires twelve independent equations of motion which fall under four different categories:

1. Force Equations $[\dot{u}, \dot{v}, \dot{w}]$
2. Moment Equations $[\dot{p}, \dot{q}, \dot{r}]$
3. Kinematic Equations $[\dot{\phi}, \dot{\theta}, \dot{\psi}]$ (Euler Rates)
4. Navigation Equations $[\dot{x}, \dot{y}, \dot{z}]$

The equations of motion for a rigid-body aircraft utilize Newton’s Second Law:

$$\sum F = m \frac{dv}{dt}$$

$\sum F$ – sum of all forces acting on the aircraft

m – aircraft mass

$\frac{dv}{dt}$ – rate of change of linear velocities

$$\sum M = \frac{d}{dt} H$$

$$H = \vec{\omega} \times I$$

$\sum M$ – sum of all moments acting on the aircraft

$\vec{\omega}$ – vector containing aircraft angular velocities

I – aircraft mass moment of inertia matrix

However, the position and orientation of an aircraft cannot be described relative to a moving body axis frame. Therefore, the body axis must go through a transformation matrix. Through making three consecutive rotations, called the “yaw-pitch-roll sequence” the following Direction Cosine Matrix (DCM) is obtained (Stevens, B. L., et. al., 2016):

$$\mathbf{R}_{NED} = \begin{bmatrix} \cos \theta \cos \psi & -\cos \phi \sin \psi + \sin \phi \sin \theta \cos \psi & \sin \phi \sin \psi + \cos \phi \sin \theta \cos \psi \\ \cos \theta \sin \psi & \cos \phi \cos \psi + \sin \phi \sin \theta \sin \psi & -\sin \phi \cos \psi + \cos \phi \sin \theta \sin \psi \\ -\sin \theta & \sin \phi \cos \theta & \cos \phi \cos \theta \end{bmatrix}$$

Once the ability to change between body and Earth reference frames is achieved, Newton’s Second Law for forces can be re-written as the force equations (1) with respect to the inertial reference frame.

$$\begin{bmatrix} \dot{u} \\ \dot{v} \\ \dot{w} \end{bmatrix} = \begin{bmatrix} rv - qw \\ pw - ru \\ qu - pv \end{bmatrix} + \begin{bmatrix} F_x/m \\ F_y/m \\ F_z/m \end{bmatrix} \quad (1)$$

$F_{x,y,z}$ – external forces acting along the x, y, or z-axis.

u, v, w – linear velocities

p, q, r – roll, pitch, and yaw rate

The external forces are typically divided into three general categories, aerodynamic, gravitational, and propulsive forces. Thus $F_i = F_{i_{Aero}} + F_{i_g} + F_{i_{Thrust}}$ for $i = x, y, z$.

Again, referencing the body to the inertial reference frame Newton's Second Law for moments yields the moment equations (2). For the inertia of the aircraft symmetry about the X-Z plane can be assumed.

$$\begin{bmatrix} \dot{p} \\ \dot{q} \\ \dot{r} \end{bmatrix} = - \begin{bmatrix} \frac{qr(I_{zz}-I_{yy})}{I_{xx}} \\ \frac{pr(I_{xx}-I_{zz})}{I_{yy}} \\ \frac{pq(I_{yy}-I_{xx})}{I_{zz}} \end{bmatrix} + \begin{bmatrix} \frac{1}{I_{xx}} & 0 & 0 \\ 0 & \frac{1}{I_{yy}} & 0 \\ 0 & 0 & \frac{1}{I_{zz}} \end{bmatrix} \begin{bmatrix} L \\ M \\ N \end{bmatrix} \quad (2)$$

L, M, N – External moments about the x, y, and z-axis

I – mass moment of inertia

Like the external forces, external moments are divided into categories of aerodynamic, gravitational, and propulsive. Therefore $L = L_{Aero} + L_g + L_{Thrust}$,

$M = M_{Aero} + M_g + M_{Thrust}$, and $N = N_{Aero} + N_g + N_{Thrust}$.

By performing a simple transformation using the Euler angles and aircraft angular rates the Euler rates, also known as the kinematic equations, can be obtained (3).

$$\begin{bmatrix} \dot{\phi} \\ \dot{\theta} \\ \dot{\psi} \end{bmatrix} = \begin{bmatrix} 1 & \sin \phi \tan \theta & \sin \phi \sec \theta \\ 0 & \cos \phi & -\sin \phi \\ 0 & \sin \phi \sec \theta & \cos \phi \sec \theta \end{bmatrix} \begin{bmatrix} p \\ q \\ r \end{bmatrix} \quad (3)$$

Through using the DCM defined and the aircraft velocities, the inertial velocities, $[\dot{x} \ \dot{y} \ \dot{z}]$, can be obtained (4). Sine and Cosine have been abbreviated to allow the equation to fit on one line.

$$\begin{bmatrix} \dot{x} \\ \dot{y} \\ \dot{z} \end{bmatrix} = \begin{bmatrix} c\theta c\psi & -c\phi s\psi + s\phi s\theta c\psi & s\phi s\psi + c\phi s\theta c\psi \\ c\theta s\psi & c\phi c\psi + s\phi s\theta s\psi & -s\phi c\psi + c\phi s\theta s\psi \\ -s\theta & s\phi c\theta & c\phi c\theta \end{bmatrix} \begin{bmatrix} u \\ v \\ w \end{bmatrix} \quad (4)$$

True airspeed (V_{TAS}), angle of attack (α), and sideslip (β) are needed to complete the

simulation. Equation (5) shows how these values are solved.

$$V_{TAS} = \sqrt{u_r^2 + v_r^2 + w_r^2}$$

$$\alpha = \tan^{-1} \left(\frac{w_r}{u_r} \right)$$

$$\beta = \sin^{-1} \left(\frac{v_r}{\sqrt{u_r^2 + v_r^2 + w_r^2}} \right)$$
(5)

$$u_r = u + u_{wind}$$

$$v_r = v + v_{wind}$$

$$w_r = w + w_{wind}$$

3.2. Aircraft Dynamics

In previous research performed at the Advanced Dynamics and Controls Lab (Lyons, Brendon. 2013), the Rascal was modeled using Digital Datcom. This provides the stability derivatives for the dynamics of the aircraft in simulation. Table 3.1 shows the values obtained previously and what is used in this thesis for simulation.

Table 3.1 Preliminary Stability Derivatives from Digital Datcom

Longitudinal Stability Derivatives (per rad)		Lateral – Directional Stability Derivatives (per rad)	
C_{L0}	0.4940	$C_{y\beta}$	-0.3198
$C_{L\alpha}$	5.9730	C_{yp}	-0.1138
C_{Lq}	4.8850	$C_{l\beta}$	-0.1002
C_{D0}	0.0310	C_{lp}	-0.5087
$C_{D\alpha}$	0.5273		
C_{m0}	0.0323	$C_{n\beta}$	0.0127
$C_{m\alpha}$	-0.3217	C_{np}	-0.0380
C_{mq}	-11.000	C_{nr}	-0.0378

After ensuring the simulation ran, the aircraft was trimmed. Table 3.2 list the values obtained.

Table 3.2 Trim Conditions for Rascal in Simulation

Parameter	Value	Units
Altitude	4563	m
Speed	38.93	m/s
Angle of Attack	-3.624	°
Elevator Deflection	5.52	°
Thrust	38.08	N

3.3. Actuator Dynamics

As described in (Lyons, Brendon 2013) Rascal engine and servos were modeled based on a first-order time-domain function. Data logged was analyzed using MATLAB's system identification tool. The transfer function for the servo was found by tracking a step in the elevator of 25° (Figure 3.3). "The Laplace transform shown in equation [6] has a time constant of 0.033 seconds (1/30) and a delay of 0.1 seconds" (Lyons, B. 2013).

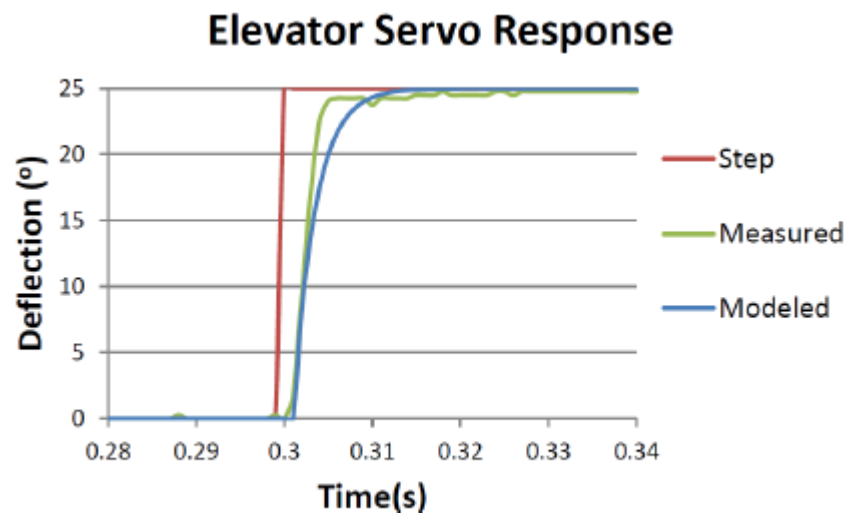


Figure 3.3 Elevator system response to a step input of 25° (Lyons, B. 2013)

$$A(s) = \frac{30}{s+30} e^{-0.1s} \quad (6)$$

Using the same method (Figure 3.4), the engine was found to have the “model shown in equation [7] as a Laplace transform with a time constant of 0.0201 seconds (1/49.75) and a delay of 0.1 seconds” (Lyons, B. 2013).

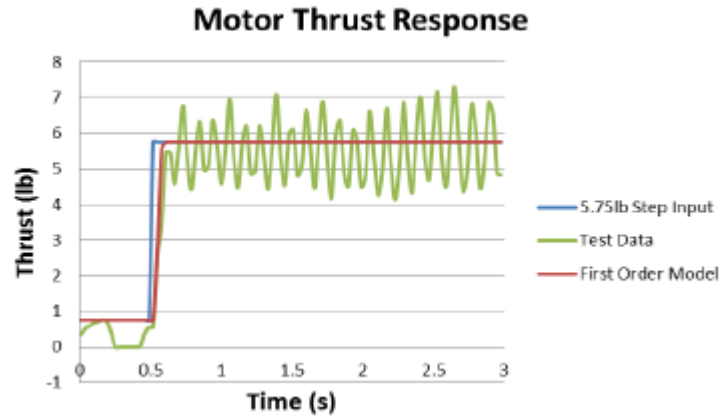


Figure 3.4 Motor System Thrust Response to 5.75 lbs. input (Lyons, B. 2013)

$$M(s) = \frac{49.75}{s+49.75} e^{-0.1s} \quad (7)$$

3.4. Aircraft Failure Model

To enable the simulation of abnormal conditions blocks have been modeled into the Rascal 110 simulation environment. After opening the model, a GUI allows the selection of control surface failures. The failure setup GUI is shown in Figure 3.5.

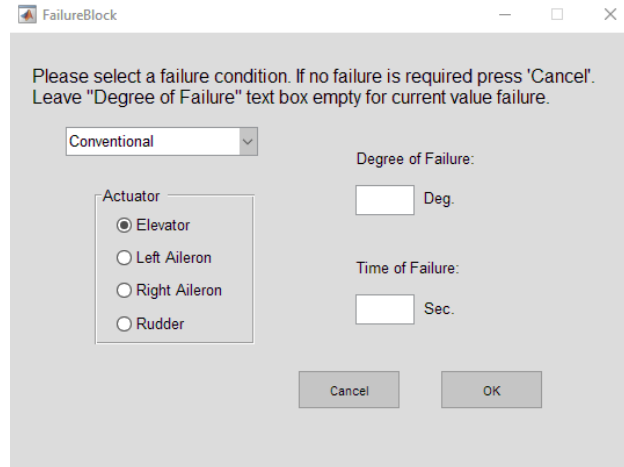


Figure 3.5 Failure setup graphical user interface (GUI)

The GUI allows the engineer to inject a failure of any degree at any time which they choose. However, through this thesis we are only interested in failures of the right aileron at 2° .

3.5. Control Architectures

Flight control systems are used to assist the pilot in operating an aircraft. Control systems “should be able to cope with non-linear and time varying nature of flight vehicles, as well as the uncertainties and un-modeled dynamics in the system and physical environment around them” (Kutluay, K. T. and Yavrucuk, I. 2010). This Thesis test two different configurations of the control system:

- Stick-to-servo – pilot has no assistance in controlling the aircraft
- Feedback linearization – also known as non-linear dynamic inversion (NLDI)

The objective is not to create a new controller but to monitor the interaction between the pilot and the control system, with a desire to see improvement in nominal operation and under failure when the pilot is assisted by the NLDI controller. The pilot closes the loop with visual tracking of the desired attitude. These attitude angles that the pilot tracks

and changes through stick deflections take time to sweep through and hence are known as the slow mode. The fast mode are the states that change rapidly, such as the angular rates. The following subsections discuss the pilot reference model and implementation of the non-linear dynamic inversion.

3.5.1. Pilot Reference Model

To give the pilot ideal handling like that of an actual aircraft, a reference model is used. A pilot reference model architecture like that presented by Perez et. al. (2015) is used to take the stick commands from the pilot $[\delta_{lat_s}, \delta_{long_s}, \delta_{dir_s}]$ and generate desired angular rate and acceleration commands. The first step is to take the pilot stick inputs and convert them into angular rate reference commands using equations (8) - (10); This ensures a stable transition from the stick inputs to the commanded angular rates.

$$p_{com} = k_{lat}\delta_{lat_s} \quad (8)$$

$$q_{com} = k_{long}\delta_{long_s} \quad (9)$$

$$r_{com} = \frac{g}{V} (k_{dir}\delta_{dir_s} + \sin \phi) \quad (10)$$

$k_{lat}, k_{long}, k_{dir}$ – pilot stick gains

g – gravity

V – True airspeed

ϕ – bank angle

Once the angular rates are obtained they are passed through a first- and second-order model reference transfer functions. These transfer functions represent the aircraft's short period, phugoid and Dutch roll modes. The outputs of the transfer functions are reference angular rates.

$$p_{ref}(s) = \frac{1}{1+\tau_{roll}s} p_{com}(s) \quad (11)$$

$$q_{ref}(s) = \frac{\omega_{n\ pitch}^2}{s^2+2\zeta_{pitch}\omega_{n\ pitch}s+\omega_{n\ pitch}^2} q_{com}(s) \quad (12)$$

$$r_{ref}(s) = \frac{\omega_{n\ yaw}^2}{s^2+2\zeta_{yaw}\omega_{n\ yaw}s+\omega_{n\ yaw}^2} r_{com}(s) \quad (13)$$

τ_{roll} – roll rate constant

$\zeta_{pitch}, \zeta_{yaw}$ – short period and Dutch roll damping

$\omega_{n\ pitch}, \omega_{n\ yaw}$ – short period and Dutch roll natural frequency

A pseudo proportional-integral (PI) controller is used to take the reference rates to angular accelerations by the equations shown in (14), where, K_p, K_i are the constants of the PI controller. They are determined to achieve adequate stability and performance characteristics in closed-loop conditions.

$$\begin{bmatrix} \ddot{p} \\ \ddot{q} \\ \ddot{r} \end{bmatrix} = \begin{bmatrix} U_p \\ U_q \\ U_r \end{bmatrix} = \begin{bmatrix} K_{pp}(p_{ref} - p) + K_{ip} \int (p_{ref} - p) \\ K_{pq}(q_{ref} - q) + K_{iq} \int (q_{ref} - q) \\ K_{pr}(r_{ref} - r) + K_{ir} \int (r_{ref} - r) \end{bmatrix} \quad (14)$$

3.5.2. Non-Linear Dynamic Inversion

Non-Linear Dynamic Inversion (NLDI) is often used with nonlinear systems such as equation (15), where $f(x)$ and $g(x)$ are non-linear state and control functions respectively. This is because its ability to eliminate inherent nonlinearities. However, the inversion is only possible given that $g^{-1}(x)$ exists.

$$\dot{x} = f(x) + g(x)u \quad (15)$$

$$u = g^{-1}(x)[\dot{x}_{des} - f(x)] \quad (16)$$

Equation (16) shows system rates, \dot{x} , are replaced by the desired states, \dot{x}_{des} to generate the generalized control laws. The theory is if the plant is modeled accurately and $\dot{x}_{des} = \dot{x}$, then nonlinearities of the system are cancelled. For this thesis the NLDI is used to provide control surface commands, Figure 3.6 shows the general architecture for this controller with the pilot reference model.

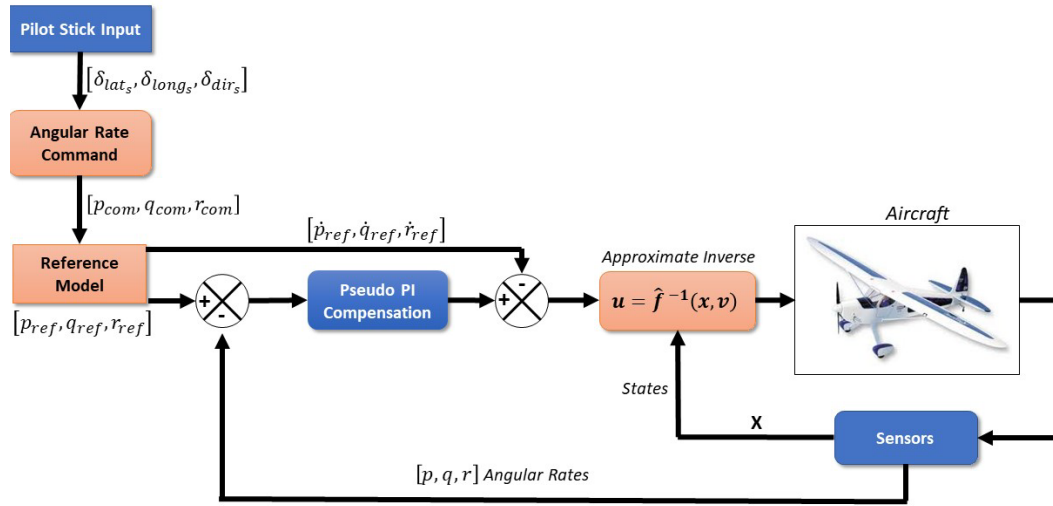


Figure 3.6 General Simulation Architecture

In this thesis NLDI is used to regulate the fast mode of the aircraft by relating the aircraft angular motion to the control surface deflections using the aerodynamic moments.

It is useful to express these moment terms as aerodynamic coefficients C_l, C_m, C_n :

$$\bar{M}_A = \begin{bmatrix} L_A \\ M_A \\ N_A \end{bmatrix} = \bar{q}S \begin{bmatrix} bC_l(x, \delta) \\ \bar{c}C_m(x, \delta) \\ bC_n(x, \delta) \end{bmatrix} \quad (17)$$

S – wing area

\bar{q} – dynamic pressure

b – wing span

\bar{c} – mean aerodynamic chord

L_A, M_A, N_A – represent the moment about their prospective axis (Figure 3.2)

δ – placeholder for relevant actuators $[\delta_a, \delta_e, \delta_r]^T$

The moments $[L_A, M_A, N_A]^T$ of equation (17) is typically written in terms of angular accelerations $[\dot{p}, \dot{q}, \dot{r}]^T$ as shown in equation (18), for convenience it is re-written here:

$$\begin{bmatrix} \dot{p} \\ \dot{q} \\ \dot{r} \end{bmatrix} = - \begin{bmatrix} \frac{qr(I_{zz}-I_{yy})}{I_{xx}} \\ \frac{pr(I_{xx}-I_{zz})}{I_{yy}} \\ \frac{pq(I_{yy}-I_{xx})}{I_{zz}} \end{bmatrix} + \begin{bmatrix} \frac{1}{I_{xx}} & 0 & 0 \\ 0 & \frac{1}{I_{yy}} & 0 \\ 0 & 0 & \frac{1}{I_{zz}} \end{bmatrix} \begin{bmatrix} L_A \\ M_A \\ N_A \end{bmatrix} \quad (18)$$

Rearranging (18) and replacing the aerodynamic moments with the desired aerodynamic moments, $[L_{A_d}, M_{A_d}, N_{A_d}]^T$ and the angular accelerations calculated in equation (14) $[U_p, U_q, U_r]^T$:

$$\begin{bmatrix} L_{A_d} \\ M_{A_d} \\ N_{A_d} \end{bmatrix} = \begin{bmatrix} qr(I_{zz} - I_{yy}) \\ pr(I_{xx} - I_{zz}) \\ pq(I_{yy} - I_{xx}) \end{bmatrix} + \begin{bmatrix} I_{xx} & 0 & 0 \\ 0 & I_{yy} & 0 \\ 0 & 0 & I_{zz} \end{bmatrix} \begin{bmatrix} U_p \\ U_q \\ U_r \end{bmatrix} \quad (19)$$

Using the standard perturbative techniques to expand the aerodynamic moment coefficient functions $[C_l(x, \delta), C_m(x, \delta), C_n(x, \delta)]^T$, they can be written as equations (20)-(22) (Lyons, B. 2013):

$$C_l(x, \delta) = C_{l_0} + C_{l_\beta} \beta + \frac{b}{2V} (C_{l_p} p + C_{l_r} r) + C_{l_{\delta a}} \delta a + C_{l_{\delta r}} \delta r \quad (20)$$

$$C_m(x, \delta) = C_{m_0} + C_{m_\alpha} \alpha + \frac{\bar{c}}{2V} C_{m_q} q + C_{m_{\delta e}} \delta e \quad (21)$$

$$C_n(x, \delta) = C_{n_0} + C_{n_\beta} \beta + \frac{b}{2V} (C_{n_p} p + C_{n_r} r) + C_{n_{\delta a}} \delta a + C_{n_{\delta r}} \delta r \quad (22)$$

Using the equations (17)-(22) the aileron, elevator, and rudder deflection commands can be found for proper tracking performance. The elevator command deflection, δe , can be obtained from the dynamic pitching moment in equation (21):

$$\delta e = \frac{C_m(x,\delta) - C_{m_0} - C_{m_\alpha} \alpha - \frac{\bar{c}}{2V} C_{m_q} q}{C_{m_{\delta e}}} = \frac{\frac{M_{A_d}}{\bar{q} S \bar{c}} - C_{m_0} - C_{m_\alpha} \alpha - \frac{\bar{c}}{2V} C_{m_q} q}{C_{m_{\delta e}}} \quad (23)$$

As can be seen in equations (20) and (22) there is coupling between the aileron and rudder deflections. To enable easier formulation of equations, the expressions in equation (24) are considered.

$$b_1 = C_{l_{\delta a}} \delta a + C_{l_{\delta r}} \delta r \text{ and } b_2 = C_{n_{\delta a}} \delta a + C_{n_{\delta r}} \delta r \quad (24)$$

Replacing equation (24) into equation (20) and (22), the following variables are obtained:

$$b_1 = C_l(x, \delta) - C_{l_0} - C_{l_\beta} \beta - \frac{b}{2V} (C_{l_p} p + C_{l_r} r) = \frac{L_{A_d}}{\bar{q} S \bar{c}} - C_{l_0} - C_{l_\beta} \beta - \frac{b}{2V} (C_{l_p} p + C_{l_r} r) \quad (25)$$

$$b_2 = C_n(x, \delta) - C_{n_0} - C_{n_\beta} \beta - \frac{b}{2V} (C_{n_p} p + C_{n_r} r) = \frac{N_{A_d}}{\bar{q} S \bar{c}} - C_{n_0} - C_{n_\beta} \beta - \frac{b}{2V} (C_{n_p} p + C_{n_r} r) \quad (26)$$

The final step is to solve for the aileron δa and rudder deflections δr . Since terms in equation (25) and (26) are known values, the resulting deflections become:

$$\delta a = \frac{C_{l_{\delta r}} b_2 - C_{n_{\delta r}} b_1}{C_{l_{\delta r}} C_{n_{\delta a}} - C_{n_{\delta r}} C_{l_{\delta a}}} \quad (27)$$

$$\delta r = \frac{C_{n_{\delta a}} b_1 - C_{l_{\delta a}} b_2}{C_{l_{\delta r}} C_{n_{\delta a}} - C_{n_{\delta r}} C_{l_{\delta a}}} \quad (28)$$

4. Pilot Induced Oscillation Metrics

In the effort to validate different control systems with analytical data, a pilot metric based on the time-domain Neal-Smith criterion is implemented. The desire with implementing a metric is to be able to “detect and prevent...unfavorable aircraft-pilot interactions” (Choe, R., et. al. 2010). This method was proposed by (Bailey, R. E. and Bidlack, T. L. 1995) and showed promising results for the predictions of flying qualities and PIO tendencies.

There are several advantages of using this time-domain Neal-Smith method. One is, “flight control nonlinearities can be evaluated without assumptions or compromise” (Bailey, R. and Bidlack, T. 1996). Therefore, analysis of the nonlinear aircraft dynamics can be conducted where in frequency-domain the model would have to be linearized. The method also allows for analysis of handling qualities when using nonlinear control laws and while under control surface failures or time-delays. While this method does have many advantages, it is not always accurate in its predictions. A previous study in manned aircraft showed a 74% success rate for the prediction of Category I PIO (Choe, R., et. al. 2010). Also depending on the size of the response window and pilot, ratings can sometimes be inconclusive. In a study by (Choe, R., et. al. 2010) a window of 5 seconds was analyzed, and pilot-in-the-loop simulation was conducted to support results. In some configurations the 5 second simulation window was able to capture the desired state with minimum oscillation, but in actual pilot-in-the-loop simulation flight after the 5 seconds the aircraft had an onset of divergence and made the plane uncontrollable. However, their results showed trends of correlation between flying qualities and piloted-simulation evaluations,

so the criterion will work as a foundation for evaluation. A broader response window of 10 seconds is also used in this thesis in hopes of better capture of handling qualities and PIO tendencies.

The basis for the time-domain Neal-Smith criterion forms from the established frequency-domain counterpart. The criterion development stems from the target step tracking task. Similar to the frequency-domain bandwidth requirement, the task performance standard is defined by acquisition time D . Variations in this acquisition time D correlate to the aggressiveness of the task. An increase in the acquisition time slows down the speed of the closed-loop response and results in a less demanding task, and vice-versa. For evaluation of the closed-loop performance the root-mean-square of the tracking error, $rms(\theta_e)$ is found. This is equivalent to the frequency-domains closed-loop resonance. Finally, in a similar manner to the frequency-domain, the pilot workload is enumerated by the pilot compensation phase angle, \angle_{pc} .

As mentioned earlier the acquisition time, D , is the time that the pilot must acquire a desired pitch attitude (Figure 4.1). D is defined as the time from the commanded step input to when pitch attitude error first becomes less than the allowable pipper error. The pipper error is set to 1/40 of the pitch attitude commanded; this is defined as an acceptable tracking error. The closed-loop performance index, $rms(\theta_e)$, is calculated over the transient response after the acquisition time D .

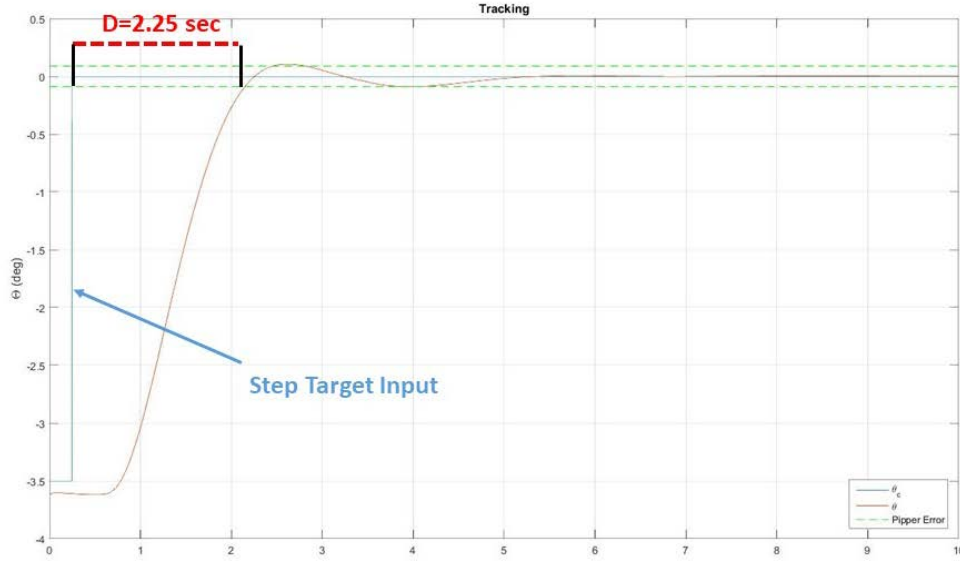


Figure 4.1 Performance Optimization Plot

In the following subsections the methods for modeling the pilot and evaluating the pilot handling qualities is explained.

4.1. Pilot Modeling

The pilot is to be tasked with tracking a simple step input for pitch, θ_c . A lead-lag transfer function, shown in equation (29), is used to model the pilot. Like that of the study conducted by Choe et. al. (2010), the transfer function is parameterized by the pilot gain, (K_p), and pilot compensation parameter (T_L). Also included in the model is a time delay, τ , which was set equal to 300 msec to represent the neuromuscular delay of the pilot (Bailey, R. and Bidlack, T. 1996). With a perfect compensator assumption, the bandwidth frequency can be written, $\omega_{BW} = \left(\frac{-1}{D-0.25} \right) * \ln \left(\frac{1}{40} \right)$.

$$\frac{\delta_p}{\theta_e}(s) = e^{-\tau s} K_p \left(\frac{\tau_{p1}s+1}{\tau_{p2}s+1} \right) \quad (29)$$

$$\tau_{p_2} = \frac{1}{\omega_{BW}} - T_L \quad (30)$$

$$\tau_{p_1} = \frac{1}{\tau_{p_2} \omega_{BW}^2} \quad (31)$$

It should be noted that the desire of this study is not to model the pilot as accurately as possible but to provide a baseline for deriving metrics that are able to accurately predict flying qualities. To obtain the values for K_p and T_L , MATLAB Simulink's optimization tool is utilized. This tool is representative of a pilot, because a pilot will attempt to adjust, and adapt to the system being controlled. The pilot is the best-case optimization because of the ability to think and adapt. The optimization tool uses defined constraints such as rise time, percent overshoot, and settling time with the objective to meet design requirements and be within the tolerances and parameter bounds (MathWorks. 2017).

For step target tracking optimization, a specified reference signal is taken as a sequence of time-amplitude pairs. The optimization tool then runs the simulation to get the simulated time-amplitude pairs. The reference and simulated time-amplitude pairs are compared to see if any match and if so a new time base is taken from their union. Then using linear interpolation, the software computes the output values and computes the scaled error. Finally, the software computes the integral square error. When this value is minimized the optimization converges.

The constraints for the optimization process for our simulation is to track a desired pitch, with the rise time being equivalent to the acquisition time, D . The optimization cost is the root-mean-square of the pitch error, $rms(\theta_e)$. Where the $rms(\theta_e)$ is computed after the acquisition time. Therefore, optimization satisfies the acquisition time, D , and simultaneously produces the minimum root-mean-squared pitch tracking error. Figure 4.2 is an optimization example after solving the optimization of the NLDI for $D = 2.25$ sec.

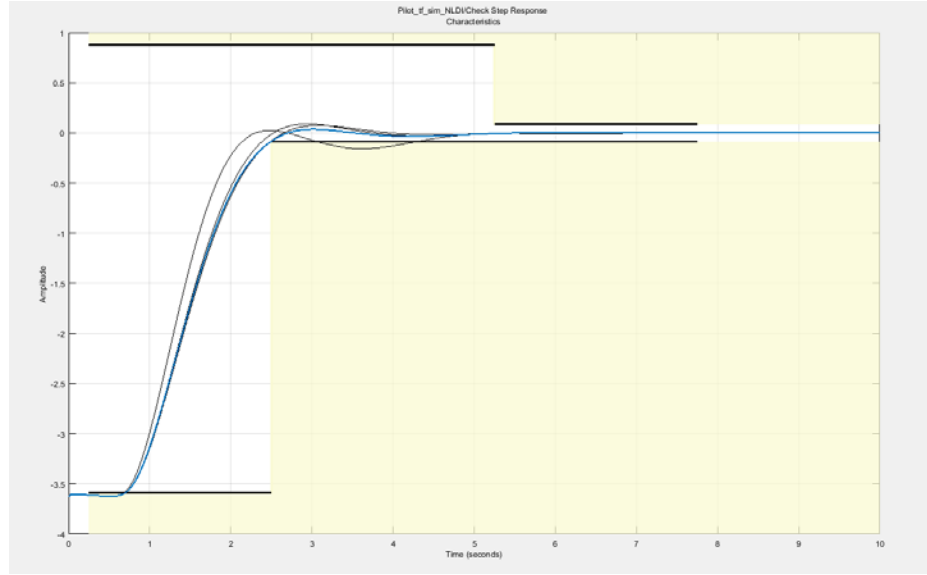


Figure 4.2 Optimization Tool Box

These optimization parameters are designed to realistically model the pilot's adaptive behavior to each aircraft configuration to “acquire the target quickly, [D] and predictably with a minimum of overshoot and oscillation, $[rms(\theta_e)]$ ” (Choe, R., et. al. 2010). Because of this flying rule and the parameters satisfying the need to “acquire quickly” and “predictably...” these serve well as performance parameters.

4.2. Flying Qualities and PIO Criterion

Pilot compensation phase angle, \angle_{pc} and root-mean-squared pitch tracking error, $rms(\theta_e)$ are used to parameterize the flying qualities in time-domain Neal-Smith criterion. The pilot compensation phase angle calculated using equation (32) represents the pilot workload. This and root-mean-squared pitch tracking error represent the closed-loop performance.

$$\angle_{pc} = \frac{180}{\pi} [\tan^{-1}(\tau_{p_1} \omega_{BW}) - \tan^{-1}(\tau_{p_2} \omega_{BW})] \quad (32)$$

For analysis these two parameters are plotted against each other after the acquisition time D in the time-domain Neal-Smith parameter plane. This parameter plane is comparable to that for frequency-domain Neal-Smith, where the only difference is \angle_{pc} is plotted against the closed-loop resonance $|\theta/\theta_c|_{max}$. In previous studies the flying qualities boundaries of the time-domain have been validated and compared to the frequency-domain ratings, also it was shown that criterion in frequency-domain mapped to a similar location on the time-domain parameter plane (Choe, R., et. al. 2010) (Bailey, R. and Bidlack, T. 1996). The time-domain Neal-Smith parameter plane boundaries shown in Figure 4.3 are related to the Cooper-Harper Rating Scale shown in Table 4.1.

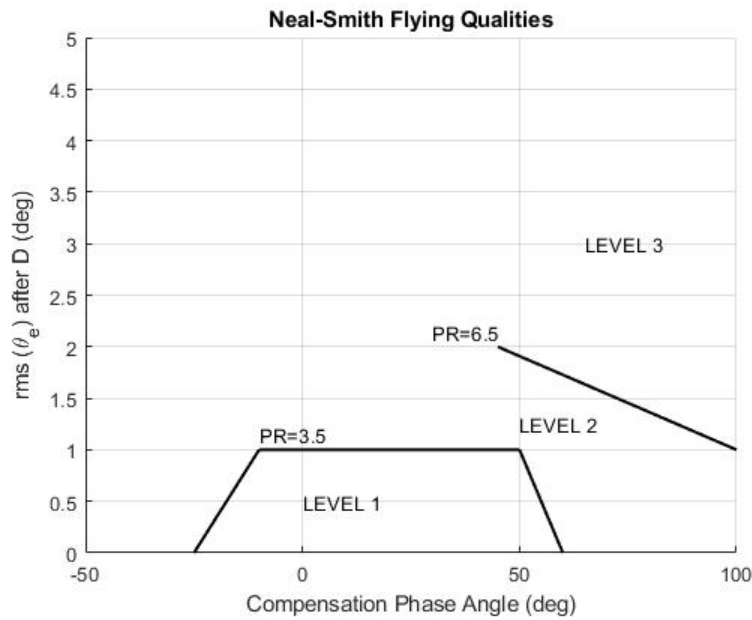


Figure 4.3 Time-Domain Neal-Smith Parameter Plane

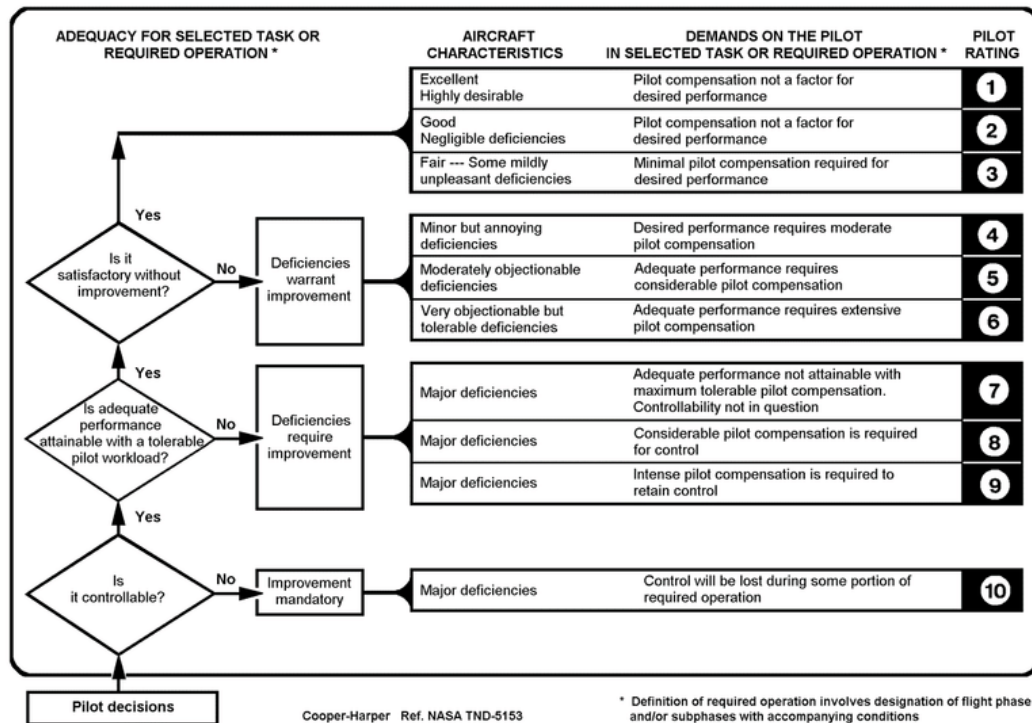


Table 4.1 Cooper-Harper Rating Scale (Cooper, G. and Harper, R. 1969)

The Cooper-Harper rating scale is what test pilots use when evaluating flight control systems based on their ability to handle and easily perform maneuvers. The scale is divided into 4 different levels:

- Level 1 are the pilot ratings from 1 to 3. This is when the aircraft is easily handled and does not ask for high demand of the pilot.
- Level 2 are the pilot ratings from 4 to 6. This aircraft is still able to be controlled but with minor and tolerable deficiencies. The pilot workload is much higher for level 2 ratings.
- Level 3 are the ratings 7 to 9. These aircraft configurations are difficult to control and require an extreme pilot workload

- Level 4 is the pilot rating of 10. This is the worst case and aircraft loss of control occurs during operation.

An additional use of the time-domain Neal-Smith criterion is the measure of whether a configuration is susceptible to pilot induced oscillations. An aircraft configuration is described as PIO-prone or -immune based on its sensitivity to task performance requirement variations. In the same way defined by Choe et. al. (2010):

The PIO criterion is formulated as: 'if local second derivative of $\text{rms}(\theta_e)$ after D with respect to D is greater than 100, the configuration is predicted to be PIO-prone. Otherwise, the configuration is predicted to be PIO-immune.'

The PIO parameter plane for time-domain Neal-Smith criterion is shown in Figure 4.4.

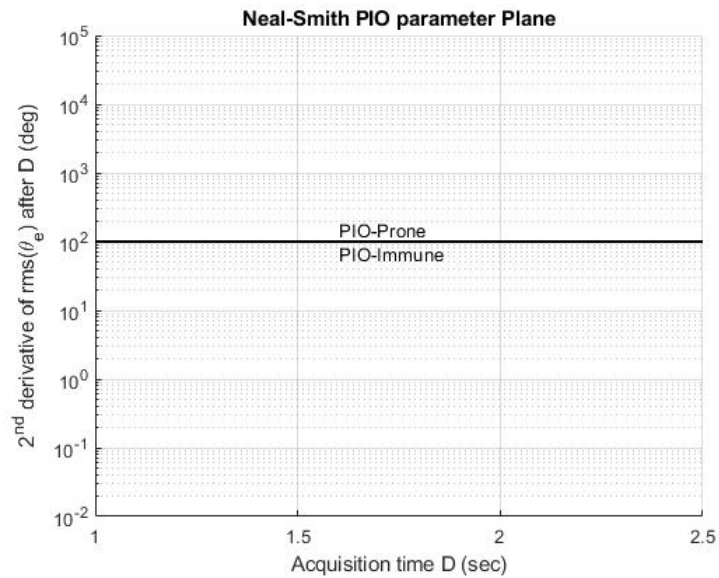


Figure 4.4 Time-Domain Neal-Smith PIO parameter plane

5. Results

In this section the results obtained from the optimization process for the prediction of flying qualities and PIO tendencies of the RPV are presented. The predictions as described in Section 4.1 are based on the time-domain Neal-Smith criteria. This chapter also presents simulation flight testing with pilot in the loop. These are to substantiate the metrics ability to evaluate a RPV's handling qualities. It is important to notice that this thesis is not focused on designing a controller for a RPV, but to generate valuable data that can be used onboard to predict flying qualities and PIO tendencies with different control configurations of a RPV.

Flight testing procedures are also explained in this Chapter as the RPV platform could be successfully operated from the GCS cockpit.

5.1. Simulation Experiments

Before performing simulations, the aircraft was trimmed and the only control that was modeled and provided was the longitudinal pitch control. The trim conditions are summarized in Table 5.1:

Table 5.1 Trim conditions for RPV simulation

Parameter	Value	Units
Altitude	4563	M
Speed	38.93	m/s
Angle of Attack	-3.624	°
Elevator Deflection	5.52	°
Thrust	38.08	N

The high altitude was chosen to allow additional time for the pilot to attempt recovery of the aircraft without crashing into the ground. Starting off with these trim states and with constant thrust value, the pilot transfer function is optimized for 5 variances in acquisition time and two different flight control configurations. The acquisition times $D = [1.25, 1.50, 1.75, 2.00, 2.25]$, and the flight control configurations are stick-to-servo and non-linear dynamic inversion. After running the optimization process, Table 5.2 is obtained.

Table 5.2 Optimized K_p, T_L with \angle_{pc} , and $rms(\theta_e)$

Control Architecture	D	K_p	T_L	\angle_{pc}	$rms(\theta_e)$
Reference NLDI	2.25	0.1053	0.0672	7.5598	0.0294
	2.00	0.1076	0.0671	8.7040	0.0303
	1.75	0.1131	0.0856	13.4187	0.0403
	1.50	0.1253	0.1044	20.6409	0.0696
	1.25	0.1446	0.1193	31.5096	0.1227
Stick To Servo	2.25	0.1884	0.0964	11.1462	0.0515
	2.00	0.1898	0.0933	12.4481	0.0530
	1.75	0.1897	0.0916	14.4678	0.0561
	1.50	0.1928	0.0915	17.7431	0.0603
	1.25	0.1832	0.0936	23.5728	0.0554

This data is then mapped to the time-domain Neal-Smith handling qualities plane to give the plots in Figure 5.1:

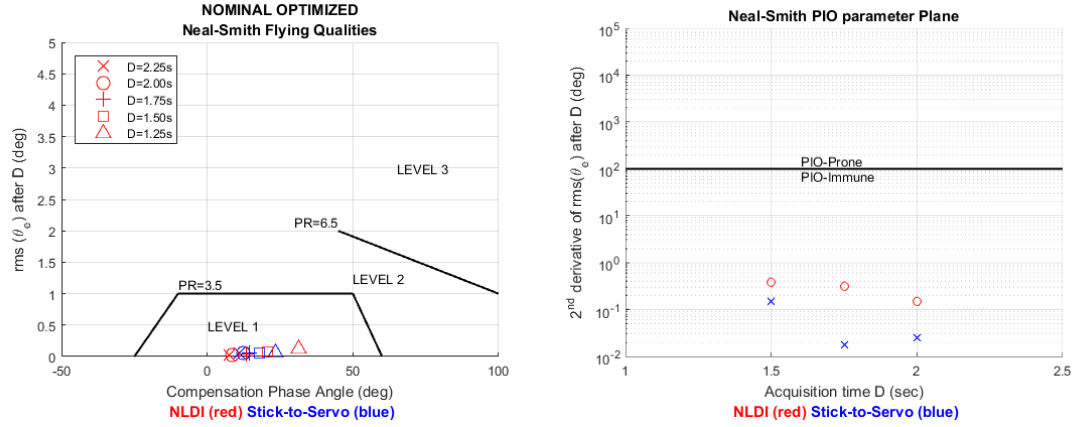


Figure 5.1 Nominal handling qualities and PIO prediction

Analyzing Figure 5.1, the optimizations of both the NLDI and the Stick-to-Servo configurations in nominal conditions are predicted to be level I handling qualities and presented an acceptable performance for all acquisition times. Since both controllers did not present sensitivity to changes in the root-mean-squared pitch error with changes in acquisition time, the resulting second derivative of the $rms(\theta_e)$ after D with respect to D is less than 100. This indicates that the configurations in nominal conditions are PIO-immune.

Figure 5.2 shows a direct time-history comparison between the NLDI and the Stick-to-Servo configuration. The NLDI shows less demand by the pilot since the elevator command is nearly half of what it required in the Stick-to-Servo configuration. This is a good sign as it means the NLDI controller is reducing the amount of workload that the pilot must produce to perform a desired maneuver.

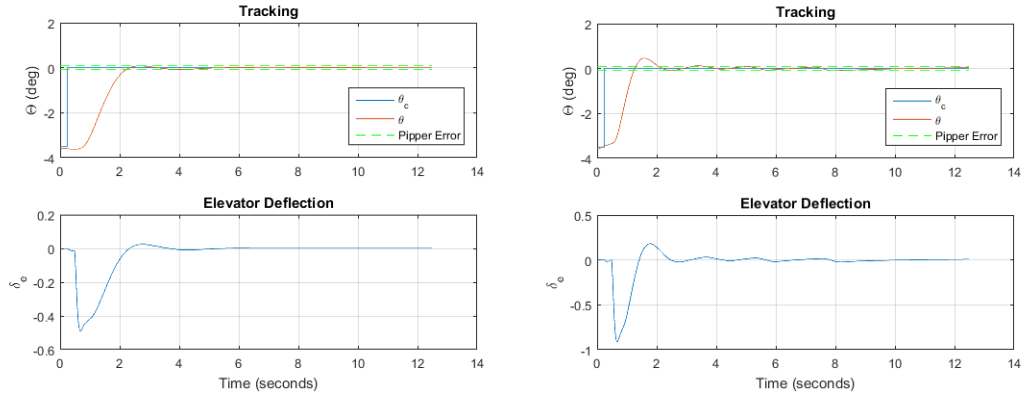


Figure 5.2 Optimization Tracking for D=2.25sec NLDI (Left) Stick-to-Servo (Right)

After optimizing in the nominal configuration, a delay of 300ms (Category I PIO) was injected. The results are shown in Figure 5.3. The pilot compensation phase angle increases for each acquisition time of both configurations. However, the stick-to-servo configuration performs better than the NLDI. This can be explained by the misrepresentation of the aircraft model reference due to the delay. The delay leads to the inversion having an additional nonlinear term which causes saturation of the control input. This is a typical issue for standard nonlinear dynamic inversion controllers which have no additional augmentation (Sieberling, S. et. al. 2010).

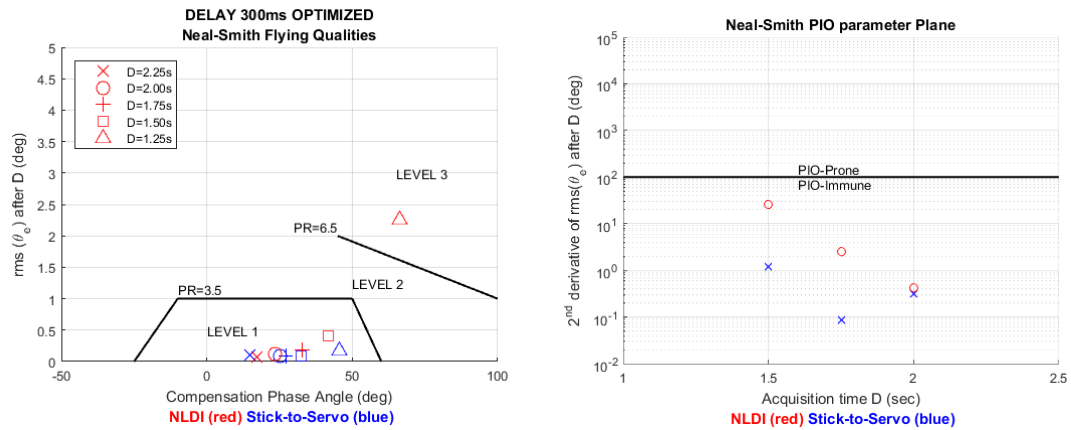


Figure 5.3 Delay 300ms handling qualities and PIO prediction

The configurations within the level I boundary show to not be susceptible to PIO. But, the NLDI with an acquisition time of 1.25 seconds did demonstrate PIO caused by the delay (Figure 5.4). It can be seen in the elevator deflection that the controls have become saturated.

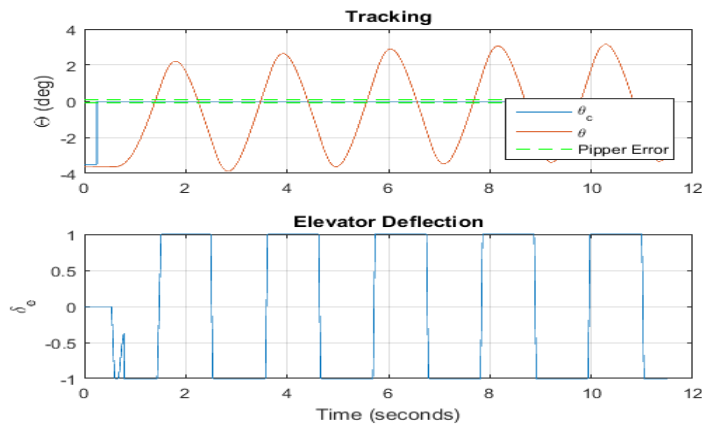


Figure 5.4 NLDI experiences PIO when a delay of 300ms present and performing an aggressive maneuver ($D=1.25$)

To test for Category II PIOs, a 2° right aileron lock is injected. The predictions are provided on the handling qualities and PIO plane in Figure 5.5. For this condition the NLDI configuration is predicted to perform better than the stick-to-servo configuration, as its root-mean-squared error is less than that of the stick-to-servo error.

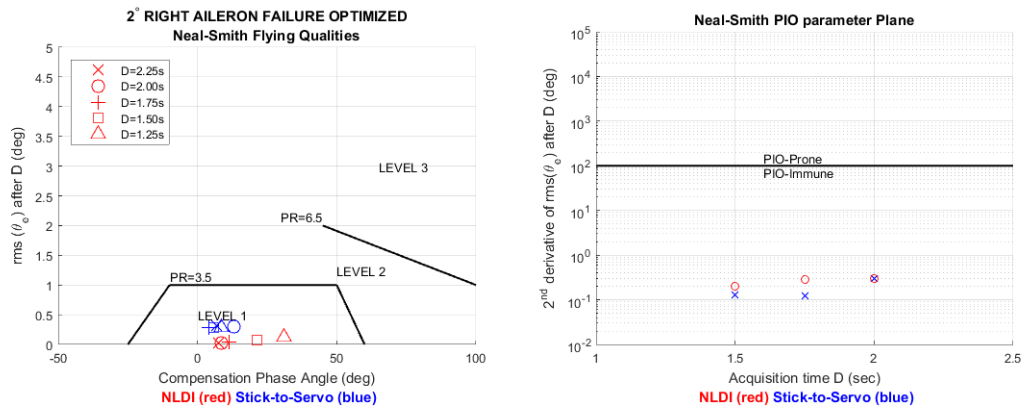


Figure 5.5 Right Aileron Lock at 2° handling qualities and PIO prediction

Following the optimizations of the pilot transfer function to predict the handling qualities, pilot-in-the-loop test were conducted. The pilot was informed at the beginning of the experiment to capture a pitch up to 0° ; the same pitch command that was done with the pilot transfer function. Figure 5.6 shows the visual provided to the pilot to acquire the pitch target in simulation.

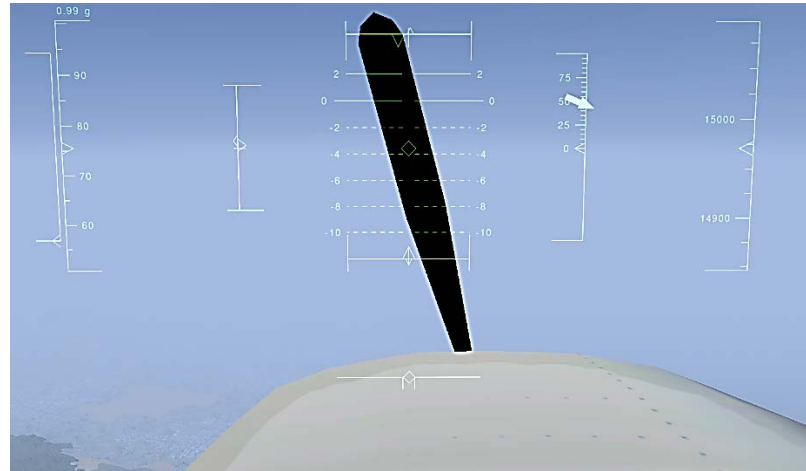


Figure 5.6 HUD used by pilot to acquire maneuver

An auditory tone and visual cue were used to inform the pilot when to start the maneuver, as shown in Figure 5.7. Once the acquisition time is up, a second audio tone sounds to indicate error values are now being collected.

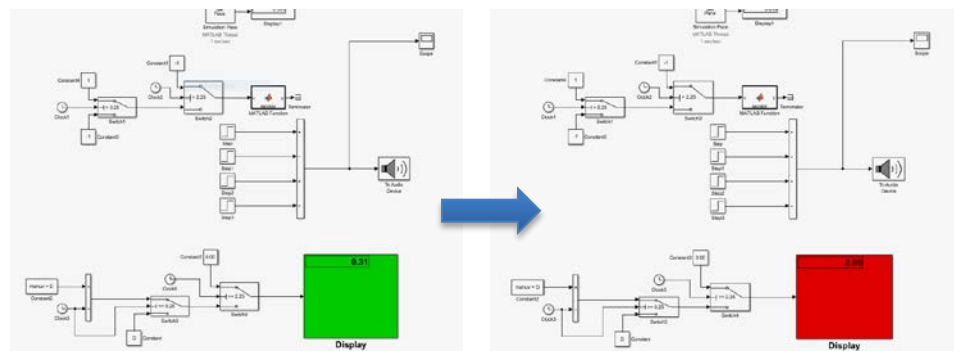


Figure 5.7 Audio and Visual Cue for Pilot to Start and Complete Maneuver

Results for tests that were executed with the Pilot-in-the-Loop are summarized in Table 5.3. The average root-mean-squared of pitch error of three different tests is taken at each acquisition time. The same pipper error $\left(\frac{1}{40}\right) \theta_c$ used with the pilot transfer function is used for the pilot-in-the-loop simulation.

Table 5.3 Pilot-in-the-Loop Experiments

Experiment	PIO Category	Conditions	Results – average $rms(\theta_e)$ in degrees					
$\theta_d = 0^\circ$ 3 tests per D			Average for D =	2.25	2.00	1.75	1.50	1.25
		Nominal	Stick-to-Servo	0.1599	0.1857	0.1812	0.2314	0.4838
			Reference NLDI	0.2184	0.1782	0.4155	0.4603	0.3862
	Category I PIO	Delay 300ms	Stick-to-Servo	0.2386	0.2087	0.1259	0.5662	0.4097
			Reference NLDI	0.9031		1.1353		2.2313
	Category II PIO	Failure at 2° right aileron	Stick-to-Servo	34.104		50.999		31.6251
			Reference NLDI	0.4597		0.8781		0.8917

During one part of the nominal experimentation the engineer did not inform the pilot that a control system was implemented. This was not done intentionally, as a pilot would normally be informed when an augmented control is in use on an aircraft. However, an adverse-pilot interaction was observed, such that the pilot was fighting the control system to converge to the desired pitch attitude. The pilot informed, “inputs were being over exaggerated,” but in fact the pilot was used to not having assistance. So, when the pilot held the yoke at the desired position in previous experiments the aircraft did not respond

in the same way, and the pilot had to continuously adjust until it was figured out what the control system was doing. Although unintentional, this anomaly was a valuable observation because it can be related to real world accidents. More specifically when an autopilot is unknowingly engaged as in Japan Airlines flight 706 in 1997, or Federal Express Flight 80 in 2009 (ALPA Japan Technical Support Team. 1997)(Japan Transportation Safety Board. 2013). The pilots and control system fighting each other caused destabilizing interaction and led to PIO which resulted in injury and loss of aircraft.

The pilots stick deflections and the pitch error are collected throughout the pilot-in-the-loop simulations. Using the error as the input and the stick deflections as the output a data set is created. Then using the MATLAB *tfest()* function a transfer function of the pilot is estimated from the data set. The *tfest()* function estimates the initial conditions using the best least squares fit and solves for the parameter values of the transfer function using the nonlinear least-squares solver. The transfer function gives a *FitPercent*, which measures how well the response of the model fits the estimation data using the normalized root mean squared error measure (MathWorks. 2017). It was desired to have a *FitPercent* of 36% or better. The time-domain Neal-Smith handling qualities plane using the pilot-in-the-loop transfer function are displayed below in Figure 5.8:

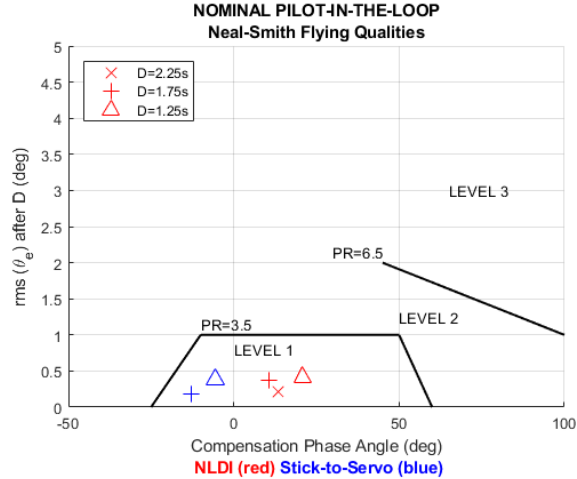


Figure 5.8 Nominal Pilot-in-the-Loop Time-Domain Handling Qualities

For nominal conditions the pilot workload was minimal, and error remain in the level one handling qualities border for both controllers (Figure 5.8). Whenever a delay of 300ms (Category I failure) was added to the system the pilot performed almost exactly as the predicted pilot transfer function optimization. Figure 5.9 shows plots of the pilot-in-the-loop elevator deflections and tracking while under a delay of 300ms and an acquisition time, $D=1.25$ s. The pilot was instructed at 6 seconds to perform the maneuver. Figure 5.10 shows the stick-to-servo configuration performs much better than the NLDI. The NLDI configuration shows actuator saturation occurring, which was predicted during the optimization in Figure 5.4.

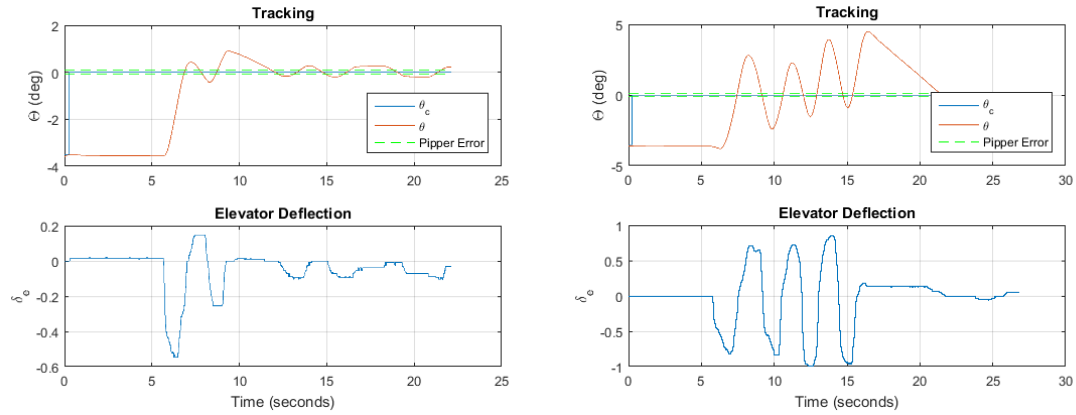


Figure 5.9 Pilot-in-the-Loop with 300ms Delay Stick-to-Servo (left) NLDI (right)

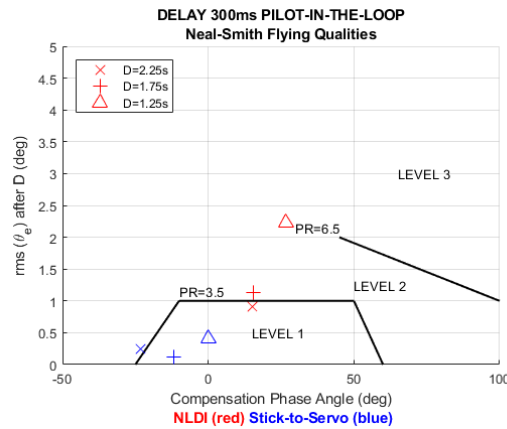


Figure 5.10 300ms Delay Pilot-in-the-Loop Time-Domain Handling Qualities

While the aircraft was under the failure of a right aileron locking at 2° , the NLDI configuration performed better than the stick-to-servo configuration. This was predicted in simulation and proved true during pilot-in-the-loop simulation. One difference, however, is that the pilot handling qualities were much worse than the prediction as shown in Figure 5.11. This can be attributed to the fact that the pilot does not know the error and takes time to figure out how to solve the problem. By the time the pilot has pinpointed the problem sometimes recovery is not possible, whereas in the transfer function simulation the problem is immediately known and attempted to be corrected. This can also explain why when under

this type of failure the simulation is rated as having level I handling qualities shown as presented in Figure 5.5.

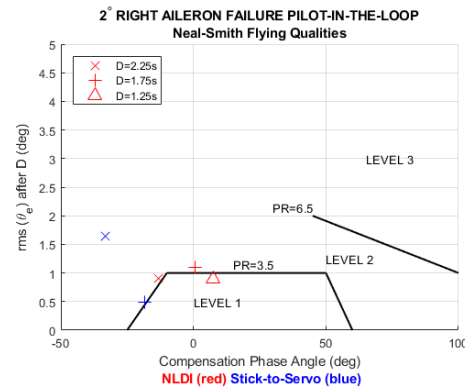


Figure 5.11 2° Right Aileron Lock Pilot-in-the-Loop Time-Domain Handling Qualities

5.2. Flight Testing

Flight Test were conducted at the Daytona Beach Radio Control Association field off Tomoka Farms Road in Port Orange (Figure 5.12).



Figure 5.12 Daytona RC Flying Park

This location offered a safe environment with reasonable space to conduct flight patterns and maneuvers. During flight test the RC pilot, GCS pilot, and engineer station all wear radios to communicate the passing of controls and any technical difficulties.

Initial flight tests were conducted over the summer of 2017 and into the spring. Prior to take off all systems are checked using both RC and GCS controls. The following pre-flight checklist is an example of the procedures followed during the flight tests:

- All battery voltages are checked to ensure enough charge for flight
- Batteries are then connected, and power switches are turned on.
- The desired code in Simulink is built, and run on the target computer using the Simulink Real-Time Explorer
- The RC pilot deflects all control surfaces ensuring they are moving in the proper direction. The on-board computer is then engaged by flipping a designated switch on the RC remote and control surfaces are checked once more.
- The RC pilot then passes control to the GCS pilot to check deflections and their direction.
- Lastly a throttle check is performed, and control is passed to the GCS pilot to ensure proper hand-off throttle on the GCS pilot controls.

Upon successful completion of the checklist the RC pilot then performs take-off and ensures that the plane is operating well, and the on-board computer is also able to receive controls and pass them through to the control surfaces. Then the RC pilot notifies the GCS pilot to be prepared to take over. The GCS pilot confirms, “Prepared for take-over” and RC pilot then enables the GCS pilot to fly. The RC pilot continues to stand by to ensure safe operation of the aircraft and to take over control if the plane is at risk. While under

control by the GCS pilot maneuvers that require the deflections of all control surfaces are performed and measured. The RC pilot then takes back control and lands the RPV.

On August 10, 2017, a short flight test was conducted using a smaller motor to check sensors, pilot visuals, and telemetry for the ground control station were working. This test was overall successful allowing about 6 minutes of flight time. The plane flew well, and the onboard computer was able to compile and feed controls through. However, the pilot visuals were not consistent and flight by the ground control station was not sustainable.

A second flight test was conducted on September 22, 2017. This configuration had the upgraded motor which is described earlier in Section 2.1 of the thesis. The flight again was to test telemetry and pilot visuals. This test lasted approximately 9 minutes. The visuals were much better than the previous flight, although noise in the visuals caused by radio interference and long-range telemetry controls made GCS flight difficult. When under the pilot cockpit controls there was large amounts of delay and the pilot was unable to maintain consistent control.

In the most recent flight on November 4, 2017, a clover leaf antenna was used for better video reception and the long-range telemetry was replaced by using trainer mode with ForceFly. These changes reduced weight as well as the amount of interference. The flight lasted approximately 9 minutes, and the pilot was able to maintain visuals until the aircraft rolled towards the ground station and signal was lost. While in straight flight the GCS pilot was able to perform roll, pitch and yaw doublets.



Figure 5.13 Flight Test at Daytona RC Flying Park

The GCS proved to be mobile and operational only needing a generator to power all equipment inside. Through preliminary flight tests, it has been proved that the RPV is operational and communicates with the GCS.

6. Conclusion and Future Work

A working platform that utilizes different types of software and hardware tools to support flight control systems testing was developed. The modified SIG Rascal 110 worked well as a remotely-piloted vehicle able to be flown from a ground station cockpit. The RPV's high-speed on-board processing system proved capable in being able to measure data and pass controls through to the aircraft. The ground control station facility performed satisfactorily, enabling different configurations to be generated and then tested on the RPV, and also allowing for the reception, and processing of data post flight.

The performance metrics based on the time-domain Neal-Smith criterion were tested in simulation and showed to be useful as a general tool, providing analytical data in reference to Cooper-Harper Rating scale. The author is aware that the simulation should be improved to more accurately represent the aerodynamic coefficients of the RPV, as this affects the handling. Nevertheless, through simulations, by analyzing the Neal-Smith flying qualities plane, the non-linear dynamic inversion control laws showed to be better under category II failure than that of the non-augmented system. The NLDI can be improved for category I failure by augmenting it with an adaptive controller.

From the research started here, future testing which implements delay to investigate PIO can be attempted. Also, more improvements and additions to the remote pilot vehicle and ground control station can continue to fit the needs of tests. A higher fidelity model for the RPV utilizing lookup tables for aerodynamic coefficients should be made. Other controllers can be investigated and implemented on-board the RPV to be tested in real-time.

Another work that would provide value to the handling qualities metric is the implementation of an Unscented Kalman Filter to predict the pilot model parameters (Mandal, T. K. and Gu, Yu). These estimated parameters could then be used to calculate the pilot compensation phase angle throughout different conditions of flight.

REFERENCES

- ALPA Japan Technical Support Team. (1997). *Japan Airlines 706 Accident Investigation Report 8 June 1997*. Over Shima Peninsula, Mie Prefecture, Japan.
- Bailey, Randall E. and Bidlack, Timothy J. (1996) *A quantitative criterion for pilot-induced oscillations – Time domain Neal-Smith criterion*. AIAA Paper 96-3434
- Bailey, R. E. and Bidlack, T. J. (1995). Unified Pilot-Induced Oscillation Theory. Volume IV: Time-Domain Neal-Smith Criterion. Tech. Rep. WL-TR-96-3031 Wright-Patterson Air Force Base, Ohio
- Belcastro, Christine M., Foster, John V., Shah, Gautam H., Gregory, Irene M., Cox, David E., Crider, Dennis A., Groff, Loren, Newman, Richard L. Klyde, David H. (2017). Aircraft Loss of Control Problem Analysis and Research Toward a Holistic Solution. *Journal of Guidance, Control, and Dynamics*, Vol. 40, No. 4, (pp. 733-775).
- Choe, Ronald, Xargay, Enric, Hovakimyan, Naira, Cao, Chengyu, Gregory, Irene M. (2010). L1 Adaptive Control under Anomaly: Flying Qualities and Adverse Pilot Interaction. *AIAA GNC Conference*. Toronto, Ontario Canada.
- Choon Seong, C. (2008). *Generic UAV Modeling to Obtain its Aerodynamic Control and Derivatives*. Monterey: Naval Post Graduate School.
- Cooper, George E., Harper Jr., Robert P. (1969) *The Use of Aircraft Pilot Rating in the Evaluation of Aircraft Handling Qualities*. NASA TN D-5153. Washington, D.C.
- Guerra, Matteo, Rhudy, Matthew, Gu, Yu, Seanor, Brad, Napolitano, Marcello R. (2012). Mobile Ground Control Station Development for Fault Tolerant UAV Research. *AIAA GNC Conference*. Minneapolis, Minnesota.
- Japan Transportation Safety Board. (2013). Aircraft Accident Investigation Report: Federal Express Corporation N526FE.
- Jordan, Thomas L. and Bailey, Roger M. (2008) Nasa Langley's AirSTAR Testbed – A Subscale Flight Test Capability for Flight Dynamics and Control System Experiments. *AIAA Guidance, Navigation, and Control Conference and Exhibit*. Honolulu, Hawaii.
- Jordan, Thomas L., Foster, John V., Bailey, Roger M., Belcastro, Christine M. (2006). AirSTAR: A UAV Platform for Flight Dynamics and Control System Testing. *25th AIAA Aerodynamic Measurement Technology and Ground Testing Conference*. San Francisco, CA.

- Kutluay, Kadriye Tiriyaki, Yavrucuk, Ilkay. (2010). Dynamic Inversion Based Control of a Missile with L1 Adaptive Control Augmentation. *IEEE International Symposium on Intelligent Control*. Yokohama, Japan.
- Larrabee, Trenton, Haiyang, Chao, Mandal, Tanmay, Gururajan, Srikanth, Gu, Yu, Napolitano, Marcello. (2013) Design, Simulation, and Flight Test Validation of a UAV Ground Control Station for Aviation Safety Research and Pilot Modeling. *AIAA GNC conference*. Boston, MA.
- Lyons, Brendon. (2013). *Performance Analysis of Non-Linear Adaptive Control Laws Using Hardware in the Loop of an Unmanned Aerial System*. Daytona Beach: Embry-Riddle Aeronautical University
- Mandal, Tanmay K., Gu, Yu. (2016). Online Pilot Model Parameter Estimation Using Sub-Scale Aircraft Flight Data. *AIAA Guidance, Navigation, and Control Conference*. San Diego, California.
- MathWorks. (2017) *Simulink Real-Time*. Retrieved from MathWorks website: <https://www.mathworks.com/products/simulink-real-time/features.html>
- MathWorks. (2017). *Design Optimization to Meet Step Response Requirements (GUI)*. Retrieved from MathWorks website: <https://www.mathworks.com/help/sldo/gs/optimize-controller-parameters-to-meet-step-response-requirements-gui.html#brz16x4-1>
- MathWorks. (2017). *Tfest*. Retrieved from MathWorks website: <https://www.mathworks.com/help/ident/ref/tfest.html>
- Mcruer, D., et. al. (1997). Aviation Safety and Pilot Control: Understanding and Preventing Unfavorable Pilot-Vehicle Interaction. The National Academies Press, Washington, D.C.
- Murch, Austin M. (2008). A Flight Control System Architecture for the NASA AirSTAR Flight Test Infrastructure. *AIAA GNC Conference and Exhibit*. Honolulu, Hawaii.
- Perez, Andres E., Moncayo, Hever, Perhinschi, Mario, Azzawi, Dia Al, Togayev, Adil. (2015). A Bio-Inspired Adaptive Control Compensation System for an Aircraft Outside Bounds of Nominal Design. *Journal of Dynamic Systems, Measurement, and Control*, Vol. 137
- Sieberling, S., Chu, Q. P., and Mulder, J. A. (2010). Robust Flight Control Using Incremental Nonlinear Dynamic Inversion and Angular Accelerations Prediction. *Journal of Guidance, Control, and Dynamics*. Vol. 33, No.6, (pp. 1732-1742)
- Stevens, Brian L., Lewis, Frank L., Johnson, Eric N. (2016). Aircraft Control and Simulation (Third ed.) Hoboken, New Jersey: John Wiley & Sons Inc.

Wilborn, James E., Foster, John V. (2004) Defining Commercial Transport Loss-of-Control: A Quantitative Approach. *AIAA Atmospheric Flight Mechanics Conference and Exhibit*. Providence, Rhode Island.

Xargay, E., Kaminer, I., Pascoal, A., Hovakimyan, N., Dobrokhodov, V., Cichella, V., Aguiar, A. P., and Ghabcheloo, R. (2013). Time-Critical Cooperative Path Following of Multiple Unmanned Aerial Vehicles over Time-Varying Networks, *Journal of Guidance, Control, and Dynamics*, Vol. 36, No. 2, (pp. 499-516).